Disentangling the chemistry and transport impacts of the Quasi-Biennial Oscillation on stratospheric ozone

Jinbo Xie[1#], Qi Tang[1], Michael Prather[2], Jadwiga Richter[3], Shixuan Zhang[4]

[1]Lawrence Livermore National Laboratory, Livermore, CA, USA

[2]Department of Earth System Science, University of California, Irvine, CA, USA

[3]National Center for Atmospheric Research, Boulder, CO, USA

[4]Pacific Northwest National Laboratory, Richmond, WA, USA

[#]now at Princeton University, New Jersey, NJ, USA

Correspondence to: Jinbo Xie (jinbo.xie@princeton.edu)

Abstract

The quasi-biennial oscillation (QBO) in tropical winds perturbs stratospheric ozone throughout much of the atmosphere via changes in transport of ozone and other trace gases and temperature changes, all of which alter ozone chemistry. Attributing these causes of the QBO-ozone variability may provide insight to model-to-model differences that contribute to ozone simulation. Here we develop a novel metric of steady-state ozone (SSO) to separate these effects: SSO calculates the local steady-state response of ozone due to the changes in temperature, chemical species, and overhead ozone column; the response due to circulation change is presumed when SSO shown no response. It is applied to the nudged Department of Energy's Energy Exascale Earth System Model version 2 (E3SMv2) with interactive ozone chemistry to demonstrate its validity. The E3SMv2 simulations nudged to reanalysis data produced reasonable wind and ozone patterns especially in the Tropics. Consistent with previous studies, we find clear demarcations with pressure. Ozone perturbations in the upper stratosphere (< 6 hPa) are predicted by the temperature changes; those between 6-hPa to 20-hPa are predicted by NO_y changes; and those in the lower stratosphere show no temperature or NO_y response and are presumably driven by circulation changes. These results are important for diagnosing model-to-model discrepancy in QBO-ozone response and enhancing reliability of ozone projections.

1. Introduction

The Quasi-Biennial Oscillation (QBO) is the principal mode of dynamical variability in the stratosphere. It is the key source of interannual variability in the overall chemical composition of the stratosphere (Randel et al., 1998; Shuckburgh et al. 2001; Park et al. 2017), manifest primarily through ozone (Reed 1964; Bowman, 1989; Wang et al., 2022).

The QBO affects ozone through both transport via atmospheric circulation and chemical processes via changed composition of the atmosphere (Reed, 1964; Holton et al., 1989; Gray and Dunkerton, 1990; Chipperfield and Gray, 1992; Chipperfield et al., 1994, Politowicz and Hitchman, 1997; Jones et al., 1998; Baldwin et al., 2001). The alternate change of QBO phase speeds up and slows down the vertical ascent in the tropics that pushes the ozone profile up and down; the QBO-temperature warms and cools the stratosphere that accelerates and decelerates ozone cycle; QBO-associated vertical transport of trace gas like reactive nitrogen reservoir NO_y may also affect ozone cycle.

Disentangling these causes of QBO-ozone variability is useful to understanding model-to-model discrepancy in the QBO-ozone simulation that contributes to improved ozone projections, such as the rate of ozone recovery that is still accompanied by large uncertainty due to internal climate variabilities like QBO (Chipperfield et al., 2017; Stone et al., 2018). Yet the role of chemical and dynamic process on QBO-ozone is still under debate (Zhang et al., 2021). Ling and London (1986) pointed to a close relationship between ozone and QBO-induced temperature anomaly and its associated photochemistry above 15-hPa. Chipperfield et al. (1994) and Tian et al. (2006) attribute the QBO-ozone to QBO modulation of NO_y species rather than the temperature changes above 10~15-hPa. Butchart et al., (2003), on the other hand, used a 3-D chemistry-climate model to argue that the transport is as important above 15~20-hPa. Currently, challenges in attributing QBO-ozone variability remain due to co-existent of chemistry and transport impact (Baldwin et al, 2001), and model limitations in simulating a free-running QBO variability (Richter et al., 2020) including asymmetry between QBO phases – a stronger and shorter QBO easterly phase and weaker and longer QBO westerly phase (Scaife et al., 2014; Richter et al., 2020). To separate the co-existent impacts, we built upon a novel use of the steady-state ozone (SSO) metric derived from the Linearized stratospheric ozone chemistry (Linoz; Mclinden et al., 2000; Hsu and Prather, 2009). The SSO assumes a "steady state" of ozone chemistry in stratosphere and is calculated in absence of dynamics, thereby isolates the

60 impacts due to chemical reactions and temperature perturbations. The determination of transport-
61 driven ozone is then based on the difference of modeled ozone from the steady-state ozone.
62 Studies have shown the validity of using linearized chemistry for representing ozone (Mclinden
63 et al., 2020) and ozone response to $4xCO_2$ (Meraner 2020), and our study build on it. The current
64 state-of-art earth system model still have problem in simulating a realistic QBO. Until now, only
65 15 of the 30 models in the Coupled Model Intercomparison Project phase 6 (CMIP6) have an
66 internally generated QBO (Richter et al., 2020). Within these models, the simulated QBO
67 amplitude and periods often fail to match the observed pattern. The World Climate Research
68 Project (WCRP) Atmospheric Processes And their Role in Climate (APARC) started an QBO
69 initiative (QBOi) in 2015 to improve Chemistry-Climate Model (CCM) simulation of tropical
70 variability (Butchart et al., 2018). The phase II of QBOi includes a set of nudging experiments to
71 examine QBO impact on climate, and here we build on those experiments.
72   In this study, we use the newly developed SSO metric on experiments following QBOi phase
73 II protocol to disentangle the chemical and transport impact of QBO on ozone. Our primary
74 modeling tool is the Department of Energy (DOE) Energy Exascale Earth Model version 2
75 (E3SMv2, Golaz et al., 2022) with interactive stratospheric ozone (Linoz v2 and Linoz v3;
76 McLinden et al., 2000; Hsu and Prather, 2009), and secondarily we examine some QBOi
77 experiments from the National Center for Atmospheric Research (NCAR) Community Earth
78 System Model (CESM). We also develop a new index of the QBO phase from a nonlinear
79 principal component analysis (NLPCA) of the tropical zonal winds that better retains asymmetric
80 patterns of QBO than standard linear PCA QBO index (Wallace et al., 1993). The phase-based
81 composite diagrams are then created to investigate the temporal evolution of ozone patterns, both
82 observed and modeled. We show that the SSO is a novel and effective tool in separating the
83 chemical and transport process of QBO on ozone, and may be applied to diagnose the model-to-
84 model discrepancy in QBO-ozone response. The observational data and ozone modeling,
85 NLPCA method, and the description of SSO are described in Sect. 2. The results are in Sect. 3.
86 The discussion and conclusion are in Sect. 4.

87 ## 2. Data and methods

88 ### 2.1 CCM models

89   The primary model for this study is E3SMv2. E3SM's atmospheric component (EAMv2) is
90 run here as a CCM with specified sea surface temperatures (SSTs) and has 72 vertical layers and

91 a horizontal resolution of about 100 km. Following Richter et al. (2010), EAMv2 employs

92 gravity wave (GW) parameterizations that include orographic GWs (McFarlane, 1987),

93 convective GWs (Beres et al., 2004), and GWs generated by frontal systems (Charron and

94 Manzini, 2002). Tunable parameters in the orographic and frontal GW parameterizations remain

95 the same as in EAMv1 (Xie et al., 2018; Rasch et al., 2019). The tunable parameters in

96 convective GWs were explored to produce a more realistic QBO in EAMv1 with a period around

97 27 months, much closer to observations (28 months) as compared to 16 months in default

98 EAMv1 (Richter et al., 2019). Nevertheless, the modeled QBO remains weak in amplitude.

99 Stratospheric ozone in E3SMv2 is calculated interactively through transport and the chemical

100 Linoz module (McLinden et al., 2000; Hsu and Prather, 2009) that was updated from the E3SM

101 O3v1 to O3v2 module (Tang et al., 2021). Linoz v2 data tables are used to calculate the 24-hour-

102 average ozone tendency (i.e., net production minus loss) from an adopted climatological mean

103 state for key species (CH_4, H_2O, and NO_y, Cl_y, Br_y) and first-order Taylor series expansions of

104 the local ozone, temperature, and overhead ozone column (see Eq. (3) in Sect. 4.1). The data

105 tables are generated for each year assuming key chemical species and families (CH_4, H_2O, and

106 NO_y, Cl_y, Br_y) follow monthly zonal-mean climatologies that scale with the slowly varying

107 changes in tropospheric mean abundance of their source gases (e.g., N_2O, CFCs, halons, CH_4,

108 tropopause H_2O). The Linoz model produces a reasonable stratospheric ozone climatology,

109 including seasonal and interannual variability and the Antarctic ozone hole (Tang et al., 2021;

110 Ruiz and Prather, 2022). The tropospheric chemical package for E3SMv2 (chemUCI) was not

111 used and the lower boundary for Linoz was set to 30 ppb. Thus, none of the ozone column

112 variability arises from tropospheric ozone chemistry. E3SMv2 diagnostics on the tendency of

113 tropospheric ozone calculate a geographically resolved stratosphere-troposphere exchange (STE)

114 flux of ozone every time step (Hsu et al., 2005; Tang et al., 2013).

115   The secondary model for this study is CESM2 (Emmons et al., 2020), using a modified

116 version of the community atmosphere model (CAM) with 83 vertical levels (Randall et al., 2023;

117 Isla et al., 2024), which is run here as a CCM with specified sea surface temperatures (SSTs).

118 CAM uses the finite-volume dynamical core with a nominal 1° horizontal resolution and with

119 physics from the Whole Atmosphere Community Climate Model version 6 (WACCM6;

120 Gettleman et al. 2019). The parameters for the convective GW momentum transport scheme is

121 tuned especially for this version to obtain a realistic, naturally generated QBO (Randall et al.,

122 2023). The inline ozone calculation in CESM2 is replaced with a monthly mean 3D ozone

123 climatology specified from a previous WACCM simulation. This input ozone forcing is formed

124 by merging WACCM simulations for historical (1850-2014, 3 members) and future period

125 (2015-2100, 1 member). As the mean of free-running CCM simulations, this ozone input

126 climatology does not have any significant QBO-like variability, and thus it cannot trigger a QBO

127 in the CCM (Butchart et al., 2023).

128 Both models are run with tropical winds being nudged to the observations and hence the

129 synchronicity of the QBO should be similar and we can compare directly with observations.

130 With the CESM2 QBO simulation we must limit our analysis to examining the forced dynamical

131 response (temperature, circulation), but with E3SM results we can compare the modeled QBO-

132 ozone interactions with observations.

133 **2.2 Observed ozone and wind**

134 For ozone, we derive the observed QBO signal from the monthly zonal mean total column

135 ozone (TCO) using the Multi-Sensor Reanalysis version 2 data (MSRv2, R.J. van der A, et al.

136 2015). This latitude-by-month dataset initially covers the period 1979-2012 and later extended to

137 2020. For stratospheric profiles, we use the zonal monthly mean latitude-by-altitude from the

138 Concentration Monthly Zonal Mean (CMZM) product (Sofieva et al., 2023). This altitude-by-

139 month profile data covers the period 1985-2020. The vertical levels are converted to pressure

140 levels inverting the pressure-altitude formula, $z^* = 16 \log_{10}(1000/P)$ km. We compared this

141 ozone data with the overlapping period from the Microwave Limb Sounder (MLS) data (V5

142 Level 3: Schwartz et al., 2021) and found only small differences with regard to QBO patterns.

143 We use ERA5 data (wind, temperature, geopotential height) from the reanalysis produced by

144 the European Center for Medium-Range Weather Forecast (ECMWF) Integrated Forecast

145 System (Hersbach et al., 2020). The version we use has 137 hybrid sigma model levels from the

146 surface to the model top at 0.01 hPa, and the horizontal resolution is about 31 km. We use

147 monthly mean data for the period 1979–2020 to analyze the QBO-related dynamical changes,

148 and 6-hourly ERA5 tropical zonal wind (15°N-15°S) to nudge model simulations mentioned

149 below. We use the 5°S-5°N tropical average zonal wind from ERA5 and simulations to

150 determinate the QBO phase index. The combined station zonal wind data from Freie University

151 of Berlin (Naujokat, 1986) for the period of 1979-2020 is also used.

152 **2.3 The QBOi simulations**

153   We use two experiments from the protocol for phase-2 of the QBOi (Butchart et al., 2018;

154   Bushell et al., 2020; Richter et al., 2020):

155   (1) Exp1-ObsQBO (E3SMv2 nudged): the zonal wind in the tropical stratosphere is

156   constrained to follow the observed QBO evolution by nudging it toward ERA5 reanalysis

157   (Hitchcock et al. 2022). Thus, the stratospheric climate including temperature and

158   circulation in the tropics is constrained.

159   (2) Exp1-AMIP (E3SMv2 natural): the zonal wind in the tropical stratosphere evolves freely

160   in each CCM being forced only by SSTs and trace-gas radiative forcing; there is no

161   nudging. The SSTs are historical and include interannual variability, primarily El Nino

162   Southern Oscillation (ENSO).

163   The nudging is applied to the zonal wind over the range 8 hPa-to-80 hPa and 15°S-to-15°N (Fig.

164   S1, nudging coefficient shown is for E3SMv2, that for CESM2 is similar). There is a slight

165   difference in how the models were nudged: E3SMv2 is nudged to the "full field" ERA5 wind

166   field including the longitudinal variability, while CESM2 is nudged to the zonally-averaged

167   ERA5 zonal wind field. The nudging relaxation timescale is 5 days. The current setup forces the

168   models to match the tropical QBO dynamic variability while allowing other variabilities to

169   evolve freely (e.g. semi-annual oscillation). For each experiment we produced 3 ensemble

170   members, and the ensemble mean is used for analysis.

171   To better understand the QBO-chemistry interactions, we performed two additional nudged

172   single-ensemble 1979-2020 runs with E3SMv2 using different chemical models: one with an

173   expanded stratospheric chemistry Linoz-v3 (referred as E3SMv2 Linoz-v3 nudged, Hsu and

174   Prather, 2010), which calculates NO_y-N_2O-CH_4-H_2O as prognostic tracers and includes their

175   interactions with ozone; a second with fixed ozone climatology as prescribed for CESM2

176   (E3SMv2 fixed-ozone nudged).

177   **2.4 NLPCA analysis of QBO phase**

178   To build a time-line composite picture of the QBO in any variable, we need to define a phase

179   of each QBO and align these phases over a 28-month period. Phase asymmetry and nonlinear

180   features of the evolution of the QBO phase are found in many studies (Lindzen and Holton 1968;

181   Holton and Lindzen, 1972; Giorgetta et al., 2002). The most obvious and sharply defined

182   synchronization point is when the QBO west phase (QBOw, i.e. prevailing westerlies) transitions

183   to the east phase (QBOe: prevailing easterlies) at some pressure level in the middle stratosphere

184   (taken as 10 hPa here) (Naujokat et al., 1986; Pahlavan et al., 2021; Kang et al., 2022). The

185   QBOe phase is typically longer (e.g., Bushell et al., 2019) with wind speeds about twice as

186   strong as that of the QBOw (Naujokat et al., 1986; Kang et al., 2022). The problem with defining

187   the QBO phase (index) simply as the month-to-month difference relative to the synchronization

188   point (e.g., Ruiz et al., 2021) is that the duration of different phases varies across successive

189   QBOs.

190   Previous use of PCA-derived QBO indices (Wallace et al., 1993) did not allow for this

191   asymmetric and nonlinear behavior. Lu et al. (2009) noted that the reconstructed wind series

192   from the PCA looked more sinusoidal in time than the actual winds, and thus the asymmetries

193   between phases did not show up in the PCA-based indices. To address these issues, we use an

194   NLPCA method that utilizes hierarchical-type neural network with an auto-associative

195   architecture (Scholz et al. 2002). It is a nonlinear generalization of the standard PCA from

196   straight lines to curves in the original data space, and natural extension to the PCA method by

197   enforcing the nonlinear components to the same hierarchical order as in the standard PCA

198   (Scholz et al., 2002). The NLPCA model described here has 5 layers with 3 hidden layers of

199   neurons. The layers of the neural-network for NLPCA are in the sequence of input-encoding-

200   bottleneck-decoding-output with the structure of n-(2k+2)-k-(2k+2)-n, where the n refers to

201   dimension of input/output dataset and k is the number of dimensions for bottleneck layer. To

202   achieve robustness, the NLPCA is applied to the tropical zonal wind data (5°S-5°N, 10-hPa to

203   70-hPa) for a set of k varying from 2 to 5, with 100 runs (different in random initialization

204   weights) for each k. The optimal number of k is set as 5 as it gives the lowest root-mean-square-

205   error between the input and output. The comparison of QBO phase angles and QBO transition

206   points are shown in Fig. S2a and S2b. It is shown that the first and second principal components

207   (PC1 and PC2) of the NLPCA account for approximately 90% of the whole variance (Figs. S2c

208   and S2d).

209   Following previous studies (Wallace et al., 1993; Hamilton and Hsieh, 2002; Lu et al., 2009),

210   the QBO phase index ψ is calculated using PC1 and PC2 as follows:

211                        $$\psi = arctan\,(v/u) \quad (-\pi \leq \psi \leq \pi\,), \quad (1)$$

212   where u and v are the time series of the PC1 and PC2, respectively. The positive/negative phase

213   angle index ψ corresponds to QBOw/QBOe.

214   We compare the reconstructed zonal wind anomalies using NLPCA and PCA (Wallace et al.,

215   1993) with the QBO cycle in the observation (Fig. 1). It is shown that the observed QBO

216   transition corresponds to an abrupt downward propagation in QBOw and a slower downward

217   transition in QBOe (indicated by clustering points in B to C to A on black triangular shape in

218   Fig. 1a). The NLPCA captures large part of this sharp transition in QBOw while PCA

219   underestimates it (indicated by points near C in Fig. 1a). This difference is also clearly shown in

220   a typical QBO cycle of 1970 September – 1972 March (Figs. 1b, 1c, and 1d, black arrow-sticks

221   exhibits the downward propagation in QBOw) and the time series of NLPCA/PCA QBO phase

222   (index) (Fig. S2).

223   NLPCA-derived QBO index is more realistic in following the atmospheric changes, it is

224   impractical to map the NLPCA phases onto the monthly-mean model diagnostics. Thus, our

225   QBO composites use simple monthly time steps about our best synchronization point, which

226   from the NLPCA analysis we take to be at the transition when phase angle index ψ crosses 0

227   with negative values before and positive values after it (from QBO easterly to QBO westerly

228   phase). It is demonstrated that comparing to QBO composites produced using the PCA-derived

229   QBO index, those that produced using the NLPCA-derived index show a shifted QBO

230   synchronization month (Fig. S2b). This results in larger contrast in observed tropical zonal wind

231   anomalies between QBOw/QBOe (Figs. S3a and S3b) that is consistent with those described in

232   previous literatures (Hamilton and Hsieh, 2002; Lu et al., 2009). This larger contrast between

233   NLPCA and PCA in zonal wind anomalies is correspondent with the larger contrast in that of the

234   total column ozone anomalies (Figs. S3c and S3d).

235   **2.5 Linoz calculation of the steady-state ozone**

236   To examine the chemical ozone response to the QBO we use the SSO calculated from both

237   Linoz v2 and v3 models. For Linoz-v2, this metric calculates local SSO response of ozone to the

238   modeled changes in temperature, chemical species, and overhead ozone column; for Linoz-v3,

239   more long-lived species are added. For Linoz v2 the SSO is derived from Eq. 4 of McLinden et

240   al. (2000). The photochemical SSO mole fraction f_{ss} (parts per million, moles per mole of dry air)

241   is expressed as follows:

242    $$f^{ss} = f^o + [(P-L)^o + \frac{\partial(P-L)}{\partial T}|^o (T-T^o) + \frac{\partial(P-L)}{\partial C_{O_3}}|^o (C_{O_3} - C_{O_3}^o)]\tau, \qquad (2)$$

8

243   This is derived by setting $\frac{d(P-L)}{dt} = 0$ for Eq. 1 as in McLinden et al., (2000). The values f^o,

244   T^o, and $C_{O_3}^o$ are the climatological values of local ozone, temperature, and overhead column

245   ozone tables used to calculate the Linoz tendencies. $(P–L)_o$ is the ozone net production minus

246   loss tendency and the partial derivatives are the sensitivity of the net production to temperature

247   and overhead column ozone.

248   A major assumption of Linoz v2 here is that the key chemical families (NO_y, Cl_y, Br_y) and

249   long-lived reactive gases (N_2O, CH_4, H_2O) do not change from their climatological values used

250   to generate the tables (Hsu and Prather, 2009). This steady-state calculation ignores transport

251   tendencies and thus will be apply only where the photochemistry is rapid, i.e., $\tau =$

252   $-[\frac{\partial(P-L)}{\partial f}|_o]^{-1} < 100$ days. Fig. 2 shows this Linoz v2 steady-state calculation (f_{SS}, T, τ) for

253   January and July using ERA5 monthly mean temperature.

254   An alternative version (Linoz v3) of the SSO derived from Hsu and Prather (2010) is

255   expressed as follows:

256   $$f_{ss} = f_o + [\ (P-L)_o + \frac{\partial(P-L)}{\partial T}|_o (T - T_o) + \frac{\partial(P-L)}{\partial C_{O_3}}|_o (C_{O_3} - C_{O_3}^o) + \sum_{j=1}^{j=5} \frac{\partial(P-L)}{\partial f_j}|_o (f_j - f_j^o)\ ]\tau, \quad (3)$$

257   This is similar as Eq. 2, except adds the contribution from sources of f_{N2O}, f_{NOy}, f_{CH4}, f_{H2O}. This

258   may be used to provide a more precise diagnosis of the SSO from those models that have these

259   output of chemistry species in addition to the temperature profile.

3. Impact of QBO on circulation and stratospheric ozone

261   Nudging the tropical zonal wind creates QBO-driven perturbations to the temperature and

262   residual circulation that we can diagnose in both the E3SMv2 and CESM2 runs and compare

263   with observations. For E3SMv2 with interactive ozone we are able to see the changes in ozone.

264   This also applies to the simulations with an internally generated QBO.

265   We create a similar composite of the QBO cycle using E3SMv2/CESM2 following Ruiz et

266   al., (2021) to see the full QBO cycle influence on stratospheric ozone. The time-composite is

267   created for each month starting 14 months prior and extending to 14 months after the QBO

268   transition for 1979-2020. The center of the composite is when the NLPCA-derived QBO phase

269   angle index (see Sect. 2.4) shifts from negative to positive (QBOe -> QBOw). We create

270   composites for circulation (zonal wind, temperature and residual circulation) and chemistry

271   tracers (total column ozone (TCO), ozone concentration, NO_y) as a function of QBO phase. For

272 TCO, we calculate the zonal-mean averages to produce the global map of composite; for all other

273 fields, we process the tropical (15°S-15°N) and extratropical (30°S-60°S/30°N-60°N) vertical

274 profile of regional average using latitudinal weight to produce the composites. The CESM2

275 ozone composite is not shown since its ozone is prescribed.

276   The structure for this section is as follows: we first analyze the impact of nudged QBO on

277 circulation in E3SM and CESM in Sect. 3.1, we then analyze its impact on global TCO and

278 tropical/extratropical ozone in Sect. 3.2 and 3.3. The chemistry and transport impact of QBO are

279 further analyzed using the SSO metric in Sect. 3.4. The overall performances of the models are

280 summarized in Sect. 3.5.

281 **3.1 Impact of QBO on circulation**

282   In this section, we examine the impact of nudged QBO on circulation in both E3SMv2 and

283 CESM2. We first analyze its impact on zonal wind and subsequently on temperature and residual

284 circulation (e.g. $\underline{w}^*$, which characterizes the transport impact of the Brewer-Dobson Circulation).

285   Through nudging, the anomalous tropical zonal wind (15°S-15°N) in both nudged E3SMv2

286 and CESM2 simulations exhibit a similar negative-positive-negative pattern to that of ERA5

287 from QBOe to QBOw (Fig. 3). In terms of the magnitude, E3SMv2 zonal wind's pattern above

288 6-hPa is minorly stronger than that of ERA5 and CESM2. Despite this minor difference, both

289 models overall reproduce the QBO signal in the tropical nudging regions. Correspondent to the

290 zonal wind changes shown in Fig. 3, the tropical temperature (Figs. 4a-c) in both models exhibit

291 a negative-positive-negative-positive pattern like that of ERA5. Alongside is the residual vertical

292 transport $\underline{w}^*$ that exhibits a positive-negative-positive-negative pattern, like that of ERA5 (Figs.

293 4d-f). Studies have documented the QBOe tends to relate to cooling and upward advection while

294 QBOw relates to warming and downward advection (Baldwin et al., 2001). The tropical

295 temperature and $\underline{w}^*$ results shown are thus in-phase with zonal wind change in both models.

296   In the extratropic region (30°N-60°N/30°S-60°S), the results for the zonal wind are noisier

297 (Fig. S4). The ERA5 results exhibit scattered signals of zonal wind changes for both hemispheres

298 (Fig. S4a). The two models exhibit noisy results like that of ERA5, with CESM2 closer to ERA5.

299 This is expected since the extratropics are more likely to be affected by dynamic noise from the

300 polar regions. Unlike that of the zonal wind, the temperature and residual vertical transport $\underline{w}^*$

301 results are smoother for both observation and nudged simulations. It is shown that ERA5 exhibits

302 about two cycles of positive-negative phase shift for temperature (Fig. 5a and 5d) and negative-

303 positive phase shift for w^* (Figs. 6a and 6d) from QBOe to QBOw, although southern

304 hemisphere (SH) is noisier than northern hemisphere (NH). Both models seem to have better

305 agreement with ERA5 in the NH (Figs. 5b, 5c and Figs. 6b, 6c), while E3SMv2 performs better

306 than CESM2 in the SH (Figs. 5e, 5f and Figs. 6e, 6f). Studies have documented that the QBO

307 signal in the extratropical temperature and vertical advection are at about 180° phase shift

308 relative to the tropical QBO signal (Baldwin et al., 2001). The results shown here are in-phase

309 with our nudged QBO signal in the tropics. Overall, the two models show some signals of QBO-

310 related signals outside of the regions of nudging on temperature and w^*, exhibiting the "spill-

311 over" effect of QBO nudging.

312   To sum up, nudging creates a more realistic QBO signal in both E3SMv2 and CESM2

313 especially in the tropical region. Outside of the nudging region, the "spill-over" effect of the

314 nudged QBO is seen mostly on temperature and w^* but less on the noisier zonal wind.

3.2 Impact of QBO on global TCO

316   In this section, we examine the impact of QBO on ozone using TCO reanalysis (MSRv2) and

317 E3SMv2 model simulations. The TCO composites from the E3SMv2 nudged simulation is

318 compared in Fig. 7. It is shown that the anomalous MSRv2 TCO exhibits a significant shift of

319 tripole pattern from QBOe to QBOw (Fig. 7a). The MSRv2 exhibits tri-pole pattern of

320 anomalous low TCO in the tropics and high in the extratropics during QBOe that gradually

321 transits to tri-pole pattern of anomalous high in the tropics and low in the extratropic during

322 QBOw. The magnitude of the negative in QBOe (5 DU) is lower than the positive pattern (12

323 DU) in QBOw in the tropics, indicating asymmetric phase response of TCO to QBO in the

324 tropics. The E3SMv2 nudged simulation is like MSRv2 in that it captures most of the tripole

325 patterns in both phases with similar amplitudes (Fig. 7b), indicating the impact of nudged QBO

326 on TCO is close to what observed. It is shown that the internally generated QBO variability in

327 E3SMv2 natural (Fig. S5a) only partly exhibits the patterns of MSRv2 with weaker amplitude

328 (nearly eight times weaker). Since the response of column ozone is mainly driven by the wind in

329 the lower stratosphere, this discrepancy likely indicates that the internal generated QBO is too

330 weak there. This and the good result in nudging run (Fig. 7b) indicate that nudging the tropical

331 zonal wind contributes to the modulation and enhancement of this "QBO-driven" TCO

332 variability in E3SMv2.

333   Overall, the nudged E3SMv2 simulations show "QBO-driven" TCO variability in accordance

334   to observation that is partly present in E3SMv2 natural simulations and enhanced by QBO

335   nudging.

3.3 Impact of QBO on tropical/extratropical stratospheric ozone

337   In this section, we analyze the impact of QBO on tropical (15°S-15°N) and extratropical

338   (30°S-60°S/30°N-60°N) stratospheric ozone concentration. The composites of ozone vertical

339   profile (1-hpa to 100-hPa) from E3SMv2 nudged and E3SMv2 Linoz-v3 nudged simulations are

340   compared with the CMZM satellite data (Fig. 8).

341   In the tropics, it is shown that the CMZM satellite ozone exhibits a double-peak vertical

342   structure with large ozone variations between 1~20-hPa and 20~100-hPa (Fig. 8a). Both peaks

343   shift in a sequence of negative-positive-negative from QBOe to QBOw, and the amplitude of the

344   upper peak is smaller than that of the lower peak (Fig. 8a). The E3SMv2 nudged simulation

345   captures most of the double-peak structure (Fig. 8b) with minor exceptions – the anomalous high

346   ozone in CMZM from month -14 to month -8 around 10-hPa and the anomalous low around 10-

347   hPa from month -2 to month 2 is missed. Studies have documented NO_y variations as the

348   primary drivers of ozone QBO changes around this range (Chipperfield et al., 1994; Tian et al.,

349   2006). Since nudged E3SMv2 simulation uses the Linoz-v2 where the chemical species such as

350   CH_4 or NO_y remain constant, the deficiency may be due to uncertainty in these chemical species.

351   To test this assumption, we also compared the E3SMv2 Linoz-v3 nudged simulation (with

352   chemistry of NO_y-N_2O-CH_4-H_2O included) with CMZM (Fig. 8c). It is shown that the E3SMv2

353   Linoz-v3 nudged simulation captures both missing ozone fluctuation between 6-hPa to 10-hPa in

354   E3SMv2 nudged, indicating that this missing chemistry may be responsible for this deficiency.

355   The E3SMv2 natural simulations, on the other hand, show similar double-peaked patterns but

356   with smaller amplitude (3 times weaker) and shorter period (Fig. S5b). This may be because the

357   period of internally generated QBO in E3SMv2 is ~21 years (Golaz et al., 2022). Overall, the

358   E3SMv2 nudged simulation modifies the period and enhances the QBO response in tropical

359   ozone that is mostly consistent with the CMZM weaker above 20-hPa and stronger below 20-

360   hPa.

361   This analysis is extended to the E3SMv2 nudged simulations in the extratropical region in

362   both hemispheres (30°N-60°N/30°S-60°S). Since the nudging is imposed only in the tropical

363   regions, we can further examine the impact of nudged QBO in the extratropics where it is free

364   running. Fig. 9 shows pressure-time cross-section of the extratropical (30°N-60°N/30°S-60°S)

365   ozone concentration as a function of QBO phase for CMZM satellite ozone, E3SMv2 nudged

366   and E3SMv2 Linoz-v3 nudged simulations. Unlike that of the tropics, the extratropical ozone for

367   CMZM is noisier despite an overall in-phase shift with QBO (Figs. 9a and 9d). The exception is

368   in the NH where the QBOw exhibits an extra phase shift to positive (Fig. 9a). It is shown that

369   nudged E3SMv2 simulations follow the similar positive-negative ozone phase shift in both

370   hemispheres (Figs. 9b and 9e) without the noisy phase shift in the NH. In terms of the amplitude,

371   the QBOw is similar for both hemispheres but being weaker than CMZM in QBOe. The ozone

372   change in the E3SMv2 Linoz-v3 nudged simulation tends to be similar to that of the E3SMv2

373   nudged simulation, except the amplitude in QBOw is stronger (Figs. 9c and 9f). Overall, the

374   E3SMv2 nudged and E3SMv2 Linoz-v3 nudged partly capture in-shift with QBO in extratropical

375   ozone in both hemispheres despite amplitude difference.

376   **3.4 Separating the chemistry and transport impact of QBO on ozone using**

377   **steady-state ozone**

378   In this section, we utilize the SSO (Eq. 2 and 3, see Sect. 2.5 for detail) introduced in Sect.

379   2.5 to separate the chemistry and transport impact of QBO on ozone. As a coupled system, the

380   QBO chemical and transport impacts on ozone are intertwined, making it difficult to diagnose

381   which QBO impact is more prominent to the ozone differences between model and observation

382   or among different models. Here we try to quantitatively separate these two terms with this new

383   diagnostic tool, recognizing their time scale differences. We first derive the Linoz-v2 SSO (Eq.

384   2) for E3SMv2 nudged and CESM2 nudged simulations (Fig. 10). Although ozone is prescribed

385   in CESM2, the SSO for CESM2 shown here is the temperature-ozone impact due to the CESM2

386   temperature profiles. To further analyze impact of temperature and different chemistry species

387   (NO_y, N_2O, H_2O, CH_4) in ozone simulation, the SSO using temperature only (Eq. 2) and using

388   temperature plus chemistry species (Eq. 3) are derived for E3SMv2 Linoz-v3 nudged (Fig. 11).

389   In the tropics (15°S-15°N), the Linoz-v2 SSO from E3SMv2 and CESM2 nudged exhibit an

390   apparent negative-positive-negative pattern above 20-hPa (Figs. 10a and 10d). These

391   corresponds to the temperature patterns above 20-hPa shown in the previous section (Figs. 4b

392   and 4c). This pattern in E3SMv2 is like that of the E3SMv2 ozone pattern above 20-hPa (Fig.

393   8b), indicating a temperature impact mostly above 20-hPa. Below 20-hPa, the prognostic ozone

394   in E3SMv2 correspond to the alternating $\underline{w}^*$ shift patterns (Fig. 4e). The residual meridional

395   circulation shows a weaker magnitude below 20-hPa and is thus less likely to play a major role

396   in ozone change (Fig. S6). This and the lack of response in SSO indicates the prognostic ozone

397   below 20-hPa in E3SMv2 is transport-driven. Like that of the analysis in the tropics, the

398   temperature impact in the extratropics (30°N-60°N/30°S-60°S) is stronger above 20-hPa for both

399   E3SMv2 (Figs. 10b and 10c) and CESM2 (Figs. 10e and 10f) nudged simulations. The

400   difference is that temperature in the SH (30°S-60°S) is overall noisier than that of the northern

401   hemisphere (30°N-60°N). This noisier SH SSO above 20-hPa in the nudged simulations

402   correspond to the noisier temperature for the two models (Figs. 5c and 5f), which may be largely

403   affected by stronger and noisier southern polar vortex (Fig. S7) as also documented by other

404   studies (Ribera et al., 2004). The intrusion of the polar vortex via event like sudden stratospheric

405   warming (Butler et al., 2017) may have an impact on the QBO-ozone relationship in the

406   extratropics. Below 20-hPa, the E3SMv2 nudged ozone corresponds to the $\underline{w}^*$ (Fig. 10b and

407   10e), indicating it's transport-driven. Overall, with the application of Linoz-v2 on E3SMv2

408   nudged simulation, we can partly separate the temperature-driven and transport-driven QBO-

409   ozone around the boundary of 20-hPa in both tropics and extratropics. The limit in this

410   application lies in the uncertainty in exclusion of chemistry transport such as NOy in the

411   simulations.

412   To test the sensitivity of the results to the chemistry variations, we further applied Linoz-v2

413   SSO (Eq. 2, temperature-only) and Linoz-v3 SSO (Eq. 3, temperature plus chemistry) to

414   E3SMv2 Linoz-v3 nudged simulation (Fig. 11). It is shown that the SSO including temperature

415   plus chemistry variation show better accordance with MSRv2 ozone (Figs. 8a, 9a, 9d) than

416   including temperature only especially in both the tropics (Figs. 11a, and 11d) and the extratropics

417   (Figs. 11c, 11d, 11e, and 11f). This better accordance is especially apparent between 6-hPa to 20-

418   hPa and in good accordance with the NO_y change (Fig. 12), indicating the impact of chemistry

419   variation within this height. To further examine the variable responsible for the change, we also

420   did the single specie sensitivity test (not shown). It is shown that including temperature plus NO_y

421   variation can reproduce the patterns in Figs. 11a-c. This indicates the NO_y variation an important

422   driver around 6-hPa to 20-hPa in QBO-ozone, in accordance with the previous studies

423   (Chipperfield et al., 1994; Tian et al., 2006).

424   The results here indicate demarcations of QBO-induced ozone at 6-hPa and 20-hPa. These

425   demarcations of the QBO-induced ozone at 6-hPa and 20-hPa may be due to the separation of

ozone lifetime below/above 20-hPa (Reed et al., 1964) and NO_y variation (Chipperfield et al., 1994; Tian et al., 2006). The ozone lifetime is relatively long compared with the dynamical process below 20-hPa while shortened considerably above it. The temperature affects ozone above 20-hPa (especially above 6-hPa) through ozone destruction – warmer anomalies accelerate ozone destruction, leading to correspondent ozone decrease (Wang et al., 2022), vice versa; the transport effect of QBO-related wind modulates the temperature through thermal wind balance enhancing/lessening the upward motion in the tropics (Plumb and Bell, 1982; Baldwin et al., 2001; Ribera et al., 2004; Punge et al., 2009). In the extratropics, the process is similar except that is controlled by the downward branch of QBO-induced circulation that is in 180° phase reversal with the tropics (Baldwin et al., 2001). This explains the apparent separation of transport- and chemistry-driven ozone changes above/below 20-hPa. Between 6-hPa to 20-hPa, QBO modulation of NO_y variation is shown to be an important contributor of the QBO-ozone cycle in addition to the temperature impact (Chipperfield et al., 1994). This explains the better reproduction of SSO above 20-hPa when including NO_y variation. Ozone transport, on the other hand, plays a relatively weaker role above 20-hPa. Overall, the demarcations of QBO-induced ozone shown here can be overall explained by photochemical process above 6-hPa, NO_y variation between 6-hPa and 20-hPa, and circulation change in vertical advection below 20-hPa. It is also worth mentioning that the nudged CESM2 also produces similar temperature and $\underline{w}^*$. This indicates that nudged CESM2 may produce similar prognostic ozone if Linoz were to be implemented as interactive ozone module.

3.5 Model performance in simulating QBO impact

In this sub-section, we examine the overall performance of E3SMv2 and CESM2 QBOi simulations in simulating the QBO-ozone relationship. We evaluate the pattern correlation and standard deviation of the area-weighted TCO pattern (60°S-60°N), vertically-weighted ozone concentration (15°S-15°N, 30°N-60°N, 30°S-60°S), zonal wind (15°S-15°N, 30°N-60°N, 30°S-60°S), temperature (15°S-15°N, 30°N-60°N, 30°S-60°S), and $\underline{w}^*$ (15°S-15°N, 30°N-60°N, 30°S-60°S). For ozone, only E3SMv2 results are shown since CESM2 has fixed ozone. The results are summarized in a Taylor diagram shown in Fig. 13. The observed pattern is plotted at the (1,0) reference point.

In terms of ozone (Fig. 13a), there are remarkable differences between the simulations. Overall, the E3SMSv2 nudged simulations perform the best, with the pattern correlation of all

457 four variables over 0.8 while other simulations are below 0.5. This indicates nudging realistic

458 QBO variability may increase the model performance in simulating ozone. In the extratropics,

459 the E3SMv2 nudged simulation has good pattern correlations, but the amplitude is off by over

460 1.5 times. The results for temperature, zonal wind and $\underline{w}^*$ are similar with ozone in the tropics

461 (Figs. 13b, 13c, and 13d). What's different is in the extratropics — both nudged

462 E3SMv2/CESM2 temperature, zonal wind, and $\underline{w}^*$ show better performance in NH extratropics

463 than in SH extratropics. This may be due to stronger polar vortices in SH and NH that disturb the

464 QBO signal (Ribera et al., 2004). Another difference is in the natural simulations – the tropical

465 temperature (15°S-15°N) and zonal wind signals exhibit reasonable correlations of over 0.7 in

466 zonal wind, over 0.5 in temperature. This indicates a discernable internally generated QBO

467 signal in the E3SMv2/CESM2, although it's weaker and does not extend to the extratropics.

4. Discussion and conclusion

4.1 Discussion

470 There are some interesting issues worth discussing in this section. First, the use of the SSO

471 provides an useful tool to diagnose the dynamical and chemical impact of the QBO on ozone. The

472 Linoz v2 SSO metric can be applied to all models with the minimum need of temperature profile

473 only. One caveat of this approach is that Linoz-v2 SSO neglects the potential impact of cross-over

474 chemical species such as the NO_y as in SSO that has been shown to be an important driver for

475 QBO-ozone change between 6-hPa to 20-hPa. Thus, it would be recommended to include at least

476 the NO_y output by the CCMs and include it in SSO calculation (Eq. 3) for a more precise diagnostic

477 between this height range. The QUasi-Biennial oscillation and Ozone Chemistry interactions in

478 the Atmosphere (QUOCA) proposed a new joint QBOi-CCMI project to improve understanding

479 of the QBO-ozone feedback in present-day and future climates. The tools shown here may be

480 useful to diagnose the uncertainty in QBO-ozone relationship among different model simulations

481 in this project.

482 Another noteworthy issue is the nudging employed in the current study. Nudging has been

483 adopted by models from different climate centers in the QBOi project to ensure the realistic

484 simulation of QBO through constraining the tropical climate. The different strategies of nudging

485 in these models and their effects on the QBO climate are thus needed to be analyzed with care.

486 Our study showed that the nudging overall constrains both E3SMv2 and CESM2 towards a

16

487 realistic representation of QBO-associated temperature and residual circulation field outside of the
488 nudged regions (15°S-15°N tropics). However, differences in the nudging strategies can play a
489 role in the detailed features of the zonal wind and temperature simulated by the two models. For
490 example, the extratropical zonal wind and temperature in CESM2 showed more scattered features
491 than those in E3SMv2 in our simulations. This may be partly because the full field nudging in
492 E3SMv2 nudge all zonal wavenumbers. This may pose a stronger constraint on field than the zonal
493 mean nudging in CESM2 that may nudge less spectrum of zonal wavenumbers.

494   Thirdly, our study shows the importance of including NO_y-N_2O-CH_4-H_2O chemistry in the
495 linearized ozone representation of climate model. Our study shows that the E3SMv2 Linoz v2
496 simulation with linearized ozone may underestimate the QBO-ozone amplitude above 10-hPa, as
497 also documented in Meraner et al., (2020). The E3SMv2 Linoz-v3 simulation with NO_y-N_2O-CH_4-
498 H_2O chemistry, on the other hand, improves this QBO-ozone magnitude especially between 6-hPa
499 to 10-hPa. Meraner et al., (2020) demonstrated the usefulness of linearized ozone in representing
500 ozone due to negligible computational cost, despite its deficiency in simulating QBO-ozone
501 magnitude. The inclusion of NO_y-N_2O-CH_4-H_2O chemistry may contribute to alleviating this
502 issue.

503   Last, the impact of ozone feedback on the climate in this study deems further attention. The
504 two models compared here show overall similar QBO-signal over the nudging runs despite have
505 two different ozone modules – one interactive and another non-interactive. One may question what
506 the results would be with the same modules under nudging. The sensitivity test of E3SMv2 fixed-
507 ozone nudged simulation shows that with fixed-ozone, the temperature patterns are still retained
508 although with an amplified magnitude in both the tropics and extratropics (Fig. S8). This indicates
509 a strong nudging impact, and an overall damping effect of interactive ozone in E3SMv2.

4.2 Conclusion

511   In this study, we utilize the SSO on nudged climate model simulations to separate the chemical
512 and transport response of the QBO ozone impact. We derive a new QBO phase index using the
513 NLPCA method and utilize this index to form QBO cycle composites to analyze QBO-ozone
514 relationships in observation and simulations. By analyzing the simulations from two QBOi
515 participant models (E3SMv2 and CESM2), we found that the nudged simulations can produce a
516 reasonable QBO impact in the tropics and create "spill-over" impact to the extratropical fields like
517 temperature and residual circulation. The nudged E3SMv2 simulation captures the tripole

composite pattern in the observed TCO. Nudging was also shown to improve the double-peaked vertical structure in observed ozone data between 1~20-hPa and 20~100-hPa over the tropics. In the extratropics outside of the nudging region, the nudged E3SMv2 simulated ozone tends to be overall in-phase with the observed but with magnitude difference, indicating the "spill-over" impact of nudged QBO signal.

Utilizing the SSO metric, we separated the chemical and transport response of ozone in E3SMv2 nudged to QBO. It is shown that these impacts have rather clear demarcations on both tropical and extratropical ozone response at 6-hPa and 20-hPa – chemistry impact correspondent to QBO-related temperature changes dominates the response above 6-hPa linked to photochemical processes and between 6-hPa to 20-hPa linked to NO_y variation, and transport impact related to QBO-related vertical advection dominates the response below 20-hPa. The results here are important for diagnosing model-model and model-observation differences in the QBO with free-running climate simulations, allowing us to separate chemical from circulation effects.

Stratospheric ozone is not only essential for protecting life on the Earth but also has important climate impacts. More and more studies reported the important role of ozone variations in modifying the stratospheric circulation and therefore influencing the surface climate (e.g. Xie et al., 2020). Since the QBO has relatively high predictability, considering its impacts on stratospheric ozone and subsequent atmospheric circulations may help improve the predictions of surface weather and climate (e.g., Li et al., 2023).

Despite the above studies, however, there are still caveats. The current study makes use of only one model in QBOi that has an interactive ozone feature. More models may be used in the future to examine the QBO-ozone relationship. These are to be assessed in future studies.

Data availability

The satellite data from the Copernicus Climate Change Service can be accessed at (https://cds.climate.copernicus.eu/cdsapp#!/dataset/satellite-ozone-v1?tab=form). The ERA5 data can be accessed at (https://cds.climate.copernicus.eu/cdsapp#!/dataset/reanalysis-era5-complete?tab=overview). The ChemDyg diagnostics can be accessed at (https://doi.org/10.5281/zenodo.11166488).

18

Author contribution

J.X., Q.T. designed the research; J.X. performed the E3SM simulations and wrote the manuscript. J.R. provided the CESM2 simulation. Q. T. and M.P.'s supervised the research and helped interpreting the results. All authors contributed to the scientific discussion and paper revision.

Competing interests

The authors declare that they have no conflict of interest.

Acknowledgement

577   Energy's Office of Biological and Environmental Research (BER) via NSF Interagency

578   Agreement 1844590.

Reference

Andrews, M. B., Knight, J. R., Scaife, A. A., et al.: Observed and Simulated Teleconnections Between the Stratospheric Quasi-Biennial Oscillation and Northern Hemisphere Winter Atmospheric Circulation, J. Geophys. Res., 124, 1219–1232, https://doi.org/10.1029/2018JD029368, 2019.

Andrews, D.G., J.R. Holton, and C.B. Leovy: Middle Atmosphere Dynamics. Academic Press, 489pp, 1987.

Anstey, J. A. and Shepherd, T. G.: High-latitude influence of the quasi-biennial oscillation, Q. J. Roy. Meteor. Soc., 140, 1–21, https://doi.org/10.1002/qj.2132, 2014.

Baldwin, M. P., Birner, T., Brasseur, G., et al.: 100 years of progress in understanding the stratosphere and mesosphere, Meteor. Mon.,59, 27.1–27.62, https://doi.org/10.1175/AMSMONOGRAPHSD-19-0003.1, 2019.

Baldwin, M. P., Gray, L. J., Dunkerton, T. J., et al., The quasi-biennial oscillation, Rev. Geophys., 39, 179–229, 2001.

Baldwin M. P., Tung KK., Extra-tropical QBO signals in angular momentum and wave forcing. Geophys. Res. Lett. 21: 2717–2720, 1994.

Beljaars, A. C. M., Brown, A. R., & Wood, N.: A new parameterization of turbulent orographic form drag. Quarterly Journal of the Royal Meteorological Society, 130, 1327–1347. https://doi.org/10.1256/qj.03.73, 2004.

Bowman, K. P.: Global patterns of the quasi-biennial oscillation in total ozone. *J. Atmos. Sci.,***46,** 3382–3343, 1989.

Brasseur, G., Hauglustaine, D., Walters, S., Rasch, P., Muller, J., Granier, C., & Tie, X: MOZART, a global chemical transport model for ozone and related chemical tracers 1. Model description. Journal of Geophysical Research-Atmospheres, 103(D21), 28,265–28,289. https://doi.org/10.1029/98JD02397, 1998.

Burkholder, J. B., Sander, S. P., Abbatt, J., Barker, J. R., Huie, R. E., Kolb, C. E., et al.: Chemical kinetics and photochemical data for use in atmospheric studies, evaluation no. 18, JPL Publication 15–10, Jet Propulsion Laboratory, Pasadena, CA. Retrieved from http://jpldataeval.jpl.nasa.gov, 2015.

Bushell, A. C., Anstey, J. A., Butchart, N., et al.:Evaluation of the quasi-biennial oscillation in global climate models for the SPARC QBO-initiative. *Quarterly Journal of the Royal Meteorological Society*, *148*(744), 1459-1489, 2020.

Butchart, N., Andrews, M. B., & Jones, C. D.: QBO phase synchronization in CMIP6 historical simulations attributed to ozone forcing. *Geophysical Research Letters*, 50, e2023GL104401. https://doi.org/10.1029/2023GL104401, 2023.

Butchart, N., Anstey, J. A., Hamilton, K., et al.: Overview of experiment design and comparison of models participating in phase 1 of the SPARC Quasi-Biennial Oscillation initiative (QBOi). *Geoscientific Model Development*, *11*(3), 1009-1032, 2018.

Butchart, N., Charlton-Perez, A. J., Cionni, I., et al.: Multimodel climate and variability of the stratosphere, J. Geophys. Res., 116, D05102, https://doi.org/10.1029/2010JD014995, 2011.

Butchart, N., Scaife, A.A., Austin, J., et al.: Quasi-biennial oscillation in ozone in a coupled chemistry-climate model. J. Geophys. Res.: Atmosphere 108 (D15), 4486, 2003.

Butler, A. H., Sjoberg, J. P., Seidel, D. J., Rosenlof, K. H.: A sudden stratospheric warming compendium, Earth System Science Data. 9 (1): 63–76. doi:10.5194/essd-9-63-2017.

Charron, M., and Manzini, E.: Gravity waves from fronts: Parameterization and middle atmosphere response in a general circulation model. *Journal of the Atmospheric Sciences*, 59(5), 923– 941. https://doi.org/10.1175/1520-0469(2002)059<0923:gwffpa>2.0.co;2, 2002.

Chipperfield, M. P., & Gray, L. J. : Two-dimensional model studies of the interannual variability of trace gases in the middle atmosphere. *Journal of Geophysical Research: Atmospheres*, *97*(D5), 5963-5980, 1992.

Chipperfield, M., Bekki, S., Dhomse, S. et al.: Detecting recovery of the stratospheric ozone layer. Nature 549, 211–218, 2017. https://doi.org/10.1038/nature23681

Chipperfield, M. P., Gray, L. J., Kinnersley, J. S., Zawodny, J.: A two-dimensional model study of the QBO signal in SAGE II NO2 and O3. *Geophysical research letters*, *21*(7), 589-592, 1994.

Coy, L., Wargan, K., Molod, A. M., et al.: Structure and dynamics of the quasi-biennial oscillation in MERRA-2, J. Climate, 29, 5339–5354, 2016.

Danabasoglu, G., Lamarque, J.-F., Bacmeister, J. et al.: The Community Earth System Model Version 2 (CESM2). Journal of Advances in Modeling Earth Systems,12, e2019MS001916. https://doi.org/10.1029/2019MS001916, 2020.

Dunkerton, T. J.: The role of gravity waves in the quasi-biennial oscillation, J. Geophys. Res., 102, 26,053-26,076, 1997.

Elsbury, D., Peings, Y., and Magnusdottir, G.:, Variation in the Holton-Tan effect by longitude, Q. J. Roy. Meteor. Soc., 147,1767–1787, https://doi.org/10.1002/qj.3993, 2021.

Emmons, L. K., Schwantes, R. H., Orlando, J. J., et al.: The Chemistry Mechanism in the Community Earth System Model version 2 (CESM2). Journal of Advances in Modeling Earth Systems, 12, e2019MS001882. https://doi.org/10.1029/2019MS001882, 2020.

Emmons, L. K., Hauglustaine, D. A., Müller, J. F., Carroll, M. A., Brasseur, G. P., Brunner, D., et al.: Data composites of airborne observations of tropospheric ozone and its precursors. Journal of Geophysical Research-Atmospheres, 105(D16), 20497–20538. https://doi.org/10.1029/2000jd900232, 2000.

Garfinkel, C. I., Shaw, T. A., Hartmann, D. L., and Waugh, D.W.: Does the Holton-Tan Mechanism Explain How the Quasi-Biennial Oscillation Modulates the Arctic Polar Vortex?, J. Atmos. Sci., 69, 1713–1733, https://doi.org/10.1175/JAS-D-11-0209.1, 2012.

Gettelman, A., & Morrison, H.: Advanced two-moment bulk microphysics for global models. Part I: Off-line tests and comparison with other schemes. Journal of Climate, 28, 1268–1287. https://doi.org/10.1175/JCLI-D-14-00102.1, 2015.

Giorgetta, M. A., Manzini, E., and Roeckner, E.: Forcing of the quasi-biennial oscillation from a broad spectrum of atmospheric waves. *Geophysical Research Letters*, *29*(8), 86-1, 2002.

Golaz, J.-C., Van Roekel, L. P., Zheng, X. et al. : The DOE E3SM Model version 2: Overview of the physical model and initial model evaluation. Journal of Advances in Modeling Earth Systems, 14, e2022MS003156. https://doi.org/10.1029/2022MS003156, 2022.

Golaz, J.-C., Caldwell, P. M., Van Roekel, L. P. et al.: The DOE E3SM coupled model version 1: Overview and evaluation at standard resolution. *Journal of Advances in Modeling Earth Systems*, 11(7), 2089– 2129. https://doi.org/10.1029/2018MS001603, 2019.

Golaz, J.-C., Larson, V. E., & Cotton, W. R. A PDF-based model for boundary layer clouds. Part I: Method and model description. Journal of the Atmospheric Sciences, 59, 3540–3551, 2002.

Gray, L. J., & Dunkerton, T. J.: The role of the seasonal cycle in the quasi-biennial oscillation of ozone. *Journal of Atmospheric Sciences*, *47*(20), 2429-2452, 1990.

Hamilton, K., & Hsieh, W. W.: Representation of the quasi-biennial oscillation in the tropical stratospheric wind by nonlinear principal component analysis. *Journal of Geophysical Research: Atmospheres*, *107*(D15), ACL-3, 2002.

Hamilton, K. : Interhemispheric asymmetry and annual synchronization of the ozone quasi-biennial oscillation. *Journal of Atmospheric Sciences*, *46*(7), 1019-1025, 1989.

Hansen, F., Matthes, K., and Gray, L. J.: Sensitivity of stratospheric dynamics and chemistry to QBO nudging width in the chemistryclimate model WACCM, J. Geophys. Res., 118, 10464–10474, https://doi.org/10.1002/jgrd.50812, 2013.

Hasebe, F.: Quasi-biennial oscillations of ozone and diabatic circulation in the equatorial stratosphere, *J. Atmos. Sci.*, 51, 729–745, 1994.

Hersbach H, Bell B, Berrisford P, et al.: The ERA5 global reanalysis, *Q J R Meteorol Soc*. 2020; 146: 1999–2049. https://doi.org/10.1002/qj.3803, 2020,

Hitchcock, P., Butler, A., Charlton-Perez, A., et al.: Stratospheric Nudging And Predictable Surface Impacts (SNAPSI): a protocol for investigating the role of stratospheric polar vortex disturbances in subseasonal to seasonal forecasts. *Geoscientific Model Development*, *15*(13), 5073-5092, 2022.

Hitchman, M. H., and C. B. Leovy: Estimation of the Kelvin wave contribution to the semiannual oscillation, *J. Atmos. Sci.*, 45, 1462, 1988.

Holton, J. R. and Tan, H.-C.: The quasi-biennial oscillation in the Northern Hemisphere lower stratosphere, J. Meteor. Soc. Japan.,60, 140–148, 1982.

Holton, J. R. and Tan, H.-C.: The influence of the equatorial quasi-biennial oscillation on the global circulation at 50 mb, J. Atmos. Sci., 37, 2200–2208, 1980.

Holton, J. R.: Influence of the annual cycle in meridional transport on the quasi-biennial oscillation in total ozone. *Journal of Atmospheric Sciences*, *46*(10), 1434-1439, 1989.

Holton, J. R., and R. S. Lindzen: An updated theory for the quasi-biennial cycle of the tropical stratosphere, *J Atmos. Sci.*, 29, 1076, 1972.

Horowitz, L. W., Walters, S., Mauzerall, D. L., Emmons, L. K., Rasch, P. J., Granier, C., et al.: A global simulation of tropospheric ozone and related tracers: Description and evaluation of MOZART, version 2. Journal of Geophysical Research-Atmospheres, 108(D24), 4784. https://doi.org/10.1029/2002jd002853, 2003.

Hsu, J. and Prather, M. J.: Stratospheric variability and tropospheric ozone, J. Geophys. Res.-Atmos., 114, D06102, https://doi.org/10.1029/2008JD010942, 2009.

Hsu, J., and M. J. Prather: Global long-lived chemical modes excited in a 3-D chemistry transport model: Stratospheric N_2O, NO_y, O_3 and CH_4 chemistry, *Geophys. Res. Lett.*, 37, L07805, doi:10.1029/2009GL042243, 2010.

Hsu, J., M. J. Prather, and O. Wild: Diagnosing the stratosphere-to-troposphere flux of ozone in a chemistry transport model, J. Geophys.Res., 110, D19305, doi:10.1029/2005JD006045, 2005.

Isla et al.: Toward the vertical resolution of the next generation of the Community Atmosphere Model, To be submitted, 2024.

Jones, D. B., Schneider, H. R., & McElroy, M. B.: Effects of the quasi-biennial oscillation on the zonally averaged transport of tracers. *Journal of Geophysical Research: Atmospheres*, *103*(D10), 11235-11249, 1998.

Jucker, M., Reichler, T., & Waugh, D. W.: How frequent are Antarctic sudden stratospheric warmings in present and future climate?. *Geophysical Research Letters*, *48*(11), e2021GL093215, 2021.

Kang, M. J., Chun, H. Y., Son, S. W., et al.: Role of tropical lower stratosphere winds in quasi-biennial oscillation disruptions. *Science Advances*, *8*(27), eabm7229, 2022.

Kinnersley, J. S., and Tung, K. K.: Mechanisms for the extratropical QBO in circulation and ozone. *Journal of the atmospheric sciences*, *56*(12), 1942-1962, 1999.

Kinnison, D. E., Brasseur, G. P., Walters, S., Garcia, R. R., Marsh, D. R., Sassi, F., et al.: Sensitivity of chemical tracers to meteorological parameters in the MOZART-3 chemical transport model. Journal of Geophysical Research-Atmospheres, 112(D20), D20302. https://doi.org/10.1029/2006jd007879, 2007.

Lamarque, J. F., Emmons, L. K., Hess, P. G., Kinnison, D. E., Tilmes, S., Vitt, F., et al.: CAM-chem: Description and evaluation of interactive atmospheric chemistry in the Community Earth System Model. Geoscientific Model Development, 5(2), 369–411. https://doi.org/10.5194/gmd-5-369-2012, 2012.

Larson, V. E. : CLUBB-SILHS: A parameterization of subgrid variability in the atmosphere. arXiv:1711.03675v2 [physics.ao-ph], 2017.

Lawrence, B. N. : A gravity-wave induced quasi-biennial oscillation in a three-dimensional mechanistic model. *Quarterly Journal of the Royal Meteorological Society*, *127*(576), 2005-2021, 2001.

Lee, S., Shelow, D., Thompson, A.M., Miller, S.: QBO and ENSO variability in temperature and ozone from SHADOZ, 1998–2005. J. Geophys. Res.: Atmosphere 115 (D18105), 2010.

Lee, H.-H., Tang, Q., and Prather, M.: E3SM Chemistry Diagnostics Package (ChemDyg) Version 0.1.4, Geosci. Model Dev. Discuss. [preprint], https://doi.org/10.5194/gmd-2023-203, 2024.

Leung, L. R., Bader, D. C., Taylor, M. A., and McCoy, R. B.: An introduction to the E3SM special collection: Goals, science drivers, development, and analysis. *Journal of Advances in Modeling Earth Systems*, 12, e2019MS001821, 2020. https://doi.org/10.1029/2019MS001821

Li, Y., Richter, J. H., Chen, C.-C., & Tang, Q.: A strengthened teleconnection of the quasi-biennial oscillation and tropical easterly jet in the past decades in E3SMv1. *Geophysical Research Letters*, 50, e2023GL104517. https://doi.org/10.1029/2023GL104517, 2023.

Lin, S. J., & Rood, R. B.: An explicit Flux-Form Semi-Lagrangian shallow water model on the sphere. Quarterly Journal of the Royal Meteorological Society, 123, 2477–2498.

Lindzen, R. S., and J. R. Holton (1968), A theory of the quasi-biennial oscillation, *J. Atmos. Sci.*, 25, 1095, 1997.

Logan, J. A., M. J. Prather, S. C. Wofsy, and M. B. Mcelroy: Atmospheric Chemistry - Response to Human Influence. Philos T R Soc A, 290, 187-234, 1978.

Lu, B. W., Pandolfo, L., and Hamilton, K.: Nonlinear representation of the quasi-biennial oscillation. *Journal of the atmospheric sciences*, *66*(7), 1886-1904, 2009.

Marquardt, C., & Naujokat, B.: An update of the equatorial QBO and its variability. *World Meteorological Organization-Publications-WMO TD*, *1*, 87-90, 1997.

Maycock, A. C., Randel, W. J., Steiner, A. K., Karpechko, A. Y., Christy, J., Saunders, R., et al.: Revisiting the mystery of recent stratospheric temperature trends, 2018. *Geophysical Research Letters*, 45, 9919–9933. https://doi.org/10.1029/2018GL078035

McFarlane, N. A.: The effect of orographically excited gravity wave drag on the general circulation of the lower stratosphere and troposphere. *Journal of the Atmospheric Sciences*, 44(14), 1775– 1800. https://doi.org/10.1175/1520-0469(1987)044<1775:teooeg>2.0.co;2, 1987.

McLinden, C. A., Olsen, S. C., Hannegan, B., et al.: Stratospheric ozone in 3-D models: A simple chemistry and the cross-tropopause flux, J. Geophys. Res., 105(D11), 14653–14665, doi:10.1029/2000JD900124, 2000.

Mengel, J. G., H. G. Mayr, K. L. Chan, et al.: Equatorial oscillations in the middle atmosphere generated by small-scale gravity waves, Geophys. Res. Lett., 22, 3027-3030, 1995.

Meraner, K., Rast, S., & Schmidt, H. (2020). How useful is a linear ozone parameterization for global climate modeling? Journal of Advances in Modeling Earth Systems, 12, e2019MS002003. https://doi.org/10.1029/2019MS002003

Morgenstern, O., Hegglin, M. I., Rozanov, E., et al.: Review of the global models used within phase 1 of the Chemistry–Climate Model Initiative (CCMI), Geosci. Model Dev., 10, 639–671, https://doi.org/10.5194/gmd-10-639-2017, 2017.

Naujokat, B.: An update of the observed quasi-biennial oscillation of the stratospheric winds over the tropics. J. Atmos. Sci., 43, 1873-1877, 1986.

Orbe, C., Plummer, D. A., Waugh, D. W., et al.: Description and Evaluation of the specified-dynamics experiment in the Chemistry-Climate Model Initiative , Atmos. Chem. Phys., 20, 3809–3840, https://doi.org/10.5194/acp-20-3809-2020, 2020.

Park, M., and Coauthors: Variability of stratospheric reactive nitrogen and ozone related to the QBO. J. Geophys. Res. Atmos., 122, 10 103–10 118, https://doi.org/10.1002/2017JD027061, 2017.

Pahlavan, H. A., Fu, Q., Wallace, J. M., & Kiladis, G. N.: Revisiting the quasi-biennial oscillation as seen in ERA5. Part I: Description and momentum budget. *Journal of the Atmospheric Sciences*, *78*(3), 673-691, 2021a.

Pahlavan, H. A., Wallace, J. M., Fu, Q., & Kiladis, G. N.: Revisiting the quasi-biennial oscillation as seen in ERA5. Part II: Evaluation of waves and wave forcing. Journal of the Atmospheric Sciences, 78(3), 693-707, 2021b.

Park, M., Randel, W. J., Kinnison, D. E., et al.: Variability of stratospheric reactive nitrogen and ozone related to the QBO. *Journal of Geophysical Research: Atmospheres*, *122*(18), 10-103, 2017.

Pawson,S., K. Labitzke, R. LenschowB, et al.: Climatology of the Northern Hemisphere stratosphere derived from Berlin analysesp, art 1, Monthly means, technicalr eport, Ser.A ,7(3), Freie Univ. Berlin, 1993.

PhotoComp: Chapter 6 - Stratospheric Chemistry SPARC Report No. 5 on the Evaluation of Chemistry-Climate Models 194-202, 2010.

Plumb, R. A., and R. C. Bell: A model of the quasi-biennial oscillation on an equatorial beta-plane, Q. J. R. Meteorol. Soc., 108, 335-352, 1982.

Prather, J. M., Remsberg, E. E.: The Atmospheric Effects of Stratospheric Aircraft: Report of the 1992 Models and Measurements Workshop. (M.J. Prather, E.E. Remsberg, Eds.), Satellite Beach, FL, 144+268+352 pp, 1993.

Politowicz, P. A., & Hitchman, M. H.: Exploring the effects of forcing quasi-biennial oscillations in a two-dimensional model. *Journal of Geophysical Research: Atmospheres*, *102*(D14), 16481-16497, 1997.

Randall, D. A., Tziperman, E., Branson, M. D., Richter, J. H., & Kang, W. :The QBO-MJO connection: A possible role for the SST and ENSO. *Journal of Climate*, 1-36, 2023.

Randel, W. J., & Cobb, J. B.: Coherent variations of monthly mean total ozone and lower stratospheric temperature. *Journal of Geophysical Research: Atmospheres*, *99*(D3), 5433-5447, 1994.

Randel, W. J., Wu, F., Russell, J. M., Roche, A., & Waters, J. W.: Seasonal cycles and QBO variations in stratospheric CH4 and H2O observed in UARS HALOE data. *Journal of the atmospheric sciences*, *55*(2), 163-185, 1998.

Randel, W. J., and F. Wu: Isolation of the ozone QBO in SAGE II data by singular value decomposition. *J. Atmos. Sci.,* **53,** 2546–2559, 1996.

Rasch, P. J., Xie, S., Ma, P.-L., et al.: An overview of the atmospheric component of the Energy Exascale Earth System Model. *Journal of Advances in Modeling Earth Systems*, 11(8), 2377– 2411. https://doi.org/10.1029/2019ms001629, 2019.

Reed, R.: A tentative model of the 26-month oscillation in tropical latitudes. Q. J. R. Meteorol. Soc. 90, 441–466, 1964.

Richter, J. H., Anstey, J. A., Butchart, N., Kawatani, Y., Meehl, G. A., Osprey, S., & Simpson, I. R.: Progress in simulating the quasi-biennial oscillation in CMIP models. *Journal Geophysical Research: Atmospheres*, 125, e2019JD032362. https://doi.org/10.1029/2019JD032362, 2020.

Richter, J. H., Chen, C.-C., Tang, Q., et al.: Improved simulation of the QBO in E3SMv1. *Journal of Advances in Modeling Earth Systems*, 11(11), 3403– 3418. https://doi.org/10.1029/2019MS001763, 2019.

Ruiz, D. J., Prather, M. J., Strahan, S. E., et al.: How atmospheric chemistry and transport drive surface variability of N2O and CFC-11. Journal of Geophysical Research: Atmospheres, 126, e2020JD033979. https://doi.org/10.1029/2020JD033979, (2021).

Ruiz, D. J. and M.J. Prather: From the middle stratosphere to the surface, using nitrous oxide to constrain the stratosphere–troposphere exchange of ozone, Atmos. Chem. Phys., 22, 2079– 2093, doi: 10.5194/acp-22-2079-2022, 2022.

Sander, et al. : Chemical kinetics and photochemical data for use in atmospheric studies, evaluation number 15, in JPL Publication 06-2., Jet Propul. Lab., Pasadena, Calif., 2006.

Scaife, A. A., et al. (2014), Predictability of the quasi-biennial oscillation and its northern winter teleconnection on seasonal to decadal timescales, *Geophys. Res. Lett.*, 41, 1752–1758, doi:10.1002/2013GL059160.

Scholz M. and Vigário R.: Nonlinear PCA: a new hierarchical approach, *Proceedings of the 10th European Symposium on Artificial Neural Networks (ESANN)*, pp. 439-444., 2002.

Schwartz, M., Froidevaux, L., Livesey, N., Read, W., and Fuller, R.: MLS/Aura Level 3 Monthly Binned Ozone (O3) Mixing Ratio on Assorted Grids V005, Greenbelt, MD, USA, Goddard Earth Sciences Data and Information Services Center (GES DISC) [data set], https://disc.gsfc.nasa.gov/datasets/ML3MBO3_005/summary (last access: 30 May 2024), 2021.

Scinocca, J., & Mcfarlane, N.: The parametrization of drag induced by stratified flow over anisotropic orography. Quarterly Journal of the Royal Meteorological Society, 126, 2353–2394. https://doi.org/10.1256/smsqj.56801, 2000.

Shibata, K.: Simulations of Ozone Feedback Effects on the Equatorial Quasi-Biennial Oscillation with a Chemistry–Climate Model. Climate, (9), 123. https://doi.org/10.3390/cli9080123, 2021.

Shuckburgh, E., Norton, W., Iwi, A., & Haynes, P.: Influence of the quasi-biennial oscillation on isentropic transport and mixing in the tropics and subtropics. *Journal of Geophysical Research: Atmospheres*, *106*(D13), 14327-14337, 2001.

Sofieva, V. F., Szelag, M., Tamminen, J., et al.: Updated merged SAGE-CCI-OMPS+ dataset for the evaluation of ozone trends in the stratosphere, Atmos. Meas. Tech., 16, 1881–1899, https://doi.org/10.5194/amt-16-1881-2023, 2023.

Stone, K.A., Solomon, S., Kinnison, D.E., On the identification of ozone recovery. Geophys. Res. Lett. 45, 5158–5165, 2018.

Tang, Q., Prather, M. J., Hsu, et al.: Evaluation of the interactive stratospheric ozone (O3v2) module in the E3SM version 1 Earth system model, Geosci. Model Dev., 14, 1219–1236, https://doi.org/10.5194/gmd-14-1219-2021, 2021.

Tang, Q., Golaz, J.-C., Van Roekel, L. P.: The fully coupled regionally refined model of E3SM version 2: overview of the atmosphere, land, and river results, Geosci. Model Dev., 16, 3953–3995, https://doi.org/10.5194/gmd-16-3953-2023, 2023.

Tang, Q., P. G. Hess, B. Brown-Steiner, and D. E. Kinnison : Tropospheric ozone decrease due to the Mount Pinatubo eruption: Reduced stratospheric influx, *Geophys. Res. Lett.*, 40, 5553–5558, doi:10.1002/2013GL056563, 2013.

Tian, W., Chipperfield, M.P., Gray, L.J., Zawodny, J.M.: Quasi-biennial oscillation and tracer distributions in a coupled chemistry-climate model. J. Geophys. Res.: Atmosphere 111 (D20), 2006.

Tilmes, S., Lamarque, J. F., Emmons, L. K., Kinnison, D. E., Ma, P. L., Liu, X., et al.: Description and evaluation of tropospheric chemistry and aerosols in the Community Earth System Model (CESM1.2). Geoscientific Model Development, 8(5), 1395–1426. https://doi.org/10.5194/gmd-8-1395-2015, 2015.

Tilmes, S., Lamarque, J. F., Emmons, L. K., Kinnison, D. E., Marsh, D., Garcia, R. R., et al.: Representation of the Community Earth System Model (CESM1) CAM4-chem within the Chemistry-Climate Model Initiative (CCMI). Geoscientific Model Development, 9(5), 1853–1890. https://doi.org/10.5194/gmd-9-1853-2016, 2016.

Tung, K. K., and H. Yang: Global QBO in circulation and ozone. Part I: Reexamination of observational evidence. *J. Atmos. Sci.,* **51,** 2699–2707, 1994.

Tweedy, O. V., Kramarova, N. A., Strahan, S. E., et al., (2017), Response of trace gases to the disrupted 2015–2016 quasi-biennial oscillation, Atmos. Chem. Phys., 17, 6813–6823, 2017.

van der A, R. J., Allaart, M. A. F., and Eskes, H. J.: Extended and refined multi sensor reanalysis of total ozone for the period 1970–2012, Atmos. Meas. Tech., 8, 3021–3035, https://doi.org/10.5194/amt-8-3021-2015, 2015.

Wallace, J., Panetta, R., and Estberg, J.: Representation of the equatorial stratospheric quasibiennial oscillation in EOF phase space, J. Atmos. Sci., 50, 1751–1762, https://doi.org/10.1175/1520-0469(1993)050<1751:ROTESQ>2.0.CO;2, 1993.

Wang L., Hardiman, S. C., Bett, P. E. et al.: What chance of a sudden stratospheric warming in the southern hemisphere?. Environmental Research Letters, 15 (10): 104038. doi:10.1088/1748-9326/aba8c1. ISSN 1748-9326, 2020.

Wang, W., Hong, J., Shangguan, M., et al.: Zonally asymmetric influences of the quasi-biennial oscillation on stratospheric ozone. Atmospheric Chemistry and Physics, 22(20), 13695-13711, 2022.

Watson, P. A. G. and Gray, L. J.: How Does the Quasi-Biennial Oscillation Affect the Stratospheric Polar Vortex?, J. Atmos. Sci., 71, 391–409, https://doi.org/10.1175/JAS-D-13-096.1, 2014.

Xie, F., Zhang, J., Li, X., et al.: Independent and joint influences of eastern Pacific El Niño–southern oscillation and quasi biennial oscillation on Northern Hemispheric stratospheric ozone, Int. J. Climatol., 12, 5289–5307, https://doi.org/10.1002/joc.6519, 2020.

896 Xie, S., Lin, W., Rasch, P. J., et al.: Understanding cloud and convective characteristics in
897 version 1 of the E3SM Atmosphere Model. Journal of Advances in Modeling Earth Systems,
898 10(10), 2618– 2644. https://doi.org/10.1029/2018ms001350, 2018.
899 Zhang, J., Xie, F., Ma, Z., et al.: Seasonal Evolution of the Quasibiennial Oscillation Impact on
900 the Northern Hemisphere Polar Vortex in Winter, J. Geophys. Res., 124, 12568–12586,
901 https://doi.org/10.1029/2019JD030966, 2019.
902 Zhang, J., Xie, F., Ma, Z., Zhang, C., et al.: Seasonal Evolution of the Quasibiennial Oscillation
903 Impact on the Northern Hemisphere Polar Vortex in Winter, J. Geophys. Res., 124, 12568–
904 12586, https://doi.org/10.1029/2019JD030966, 2019.
905 Zhang, R., Tian, W., and Wang, T.: Role of the quasi-biennial oscillation in the downward
906 extension of stratospheric northern annular mode anomalies, Clim. Dynam., 55, 595–612, 2019.
907 Zhang, J., Chongyang Z., Kequan Z., et al.: The role of chemical processes in the quasi-
908 biennial oscillation (QBO) signal in stratospheric ozone. Atmospheric Environment 244,
909 117906, 2021.
910
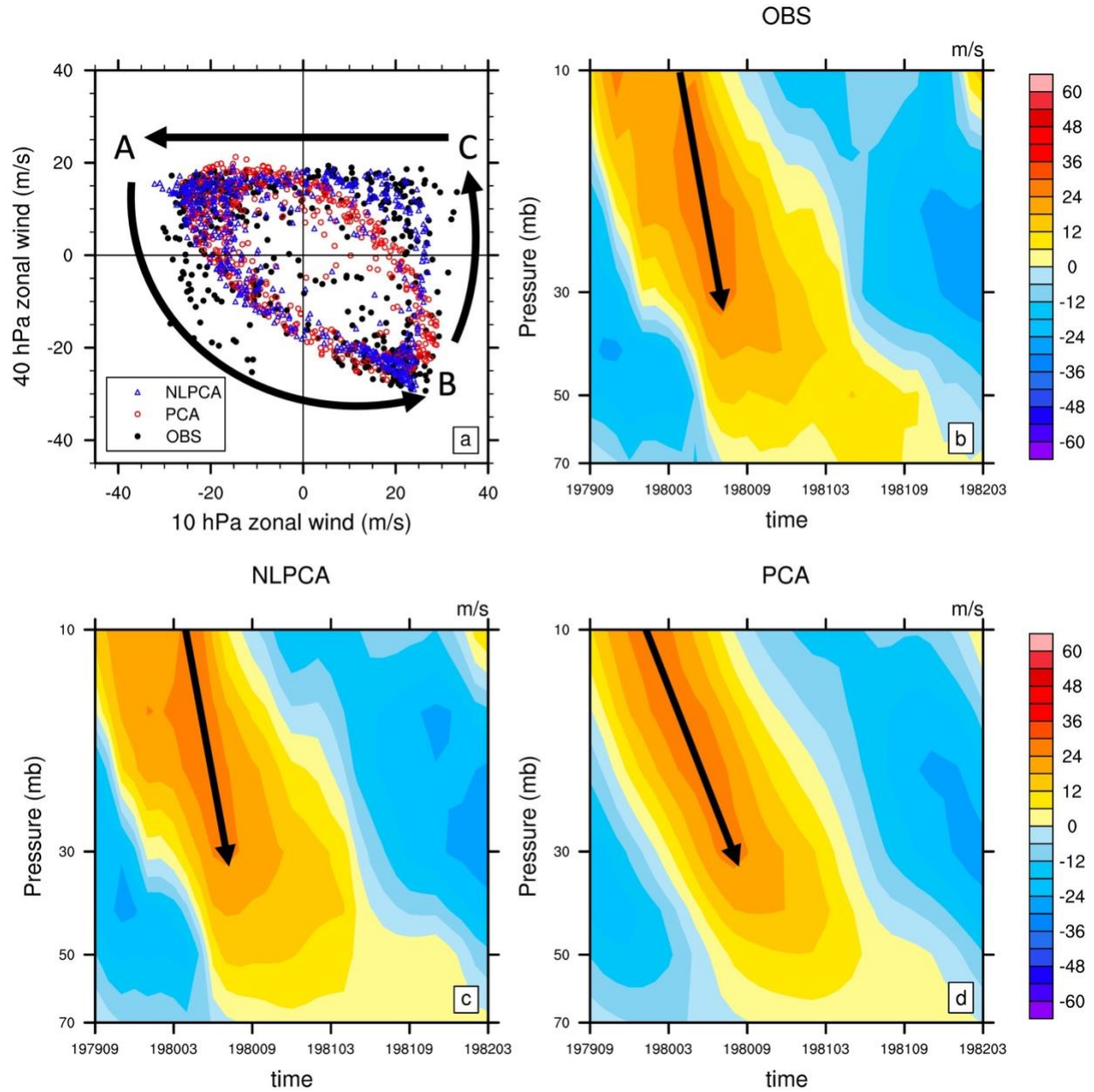
Figure 1 (a) Scatter-plot of 1979-2020 monthly mean zonal wind anomaly (m/s) at 10-hPa vs 40-hPa for observation (black), NLPCA reconstruction (blue), and PCA reconstruction (red). Typical cycle of QBO (1979 September-1982 March) from (b) Observational station data from University of Berlin, (c) NLPCA reconstruction, (d) PCA reconstruction.

29
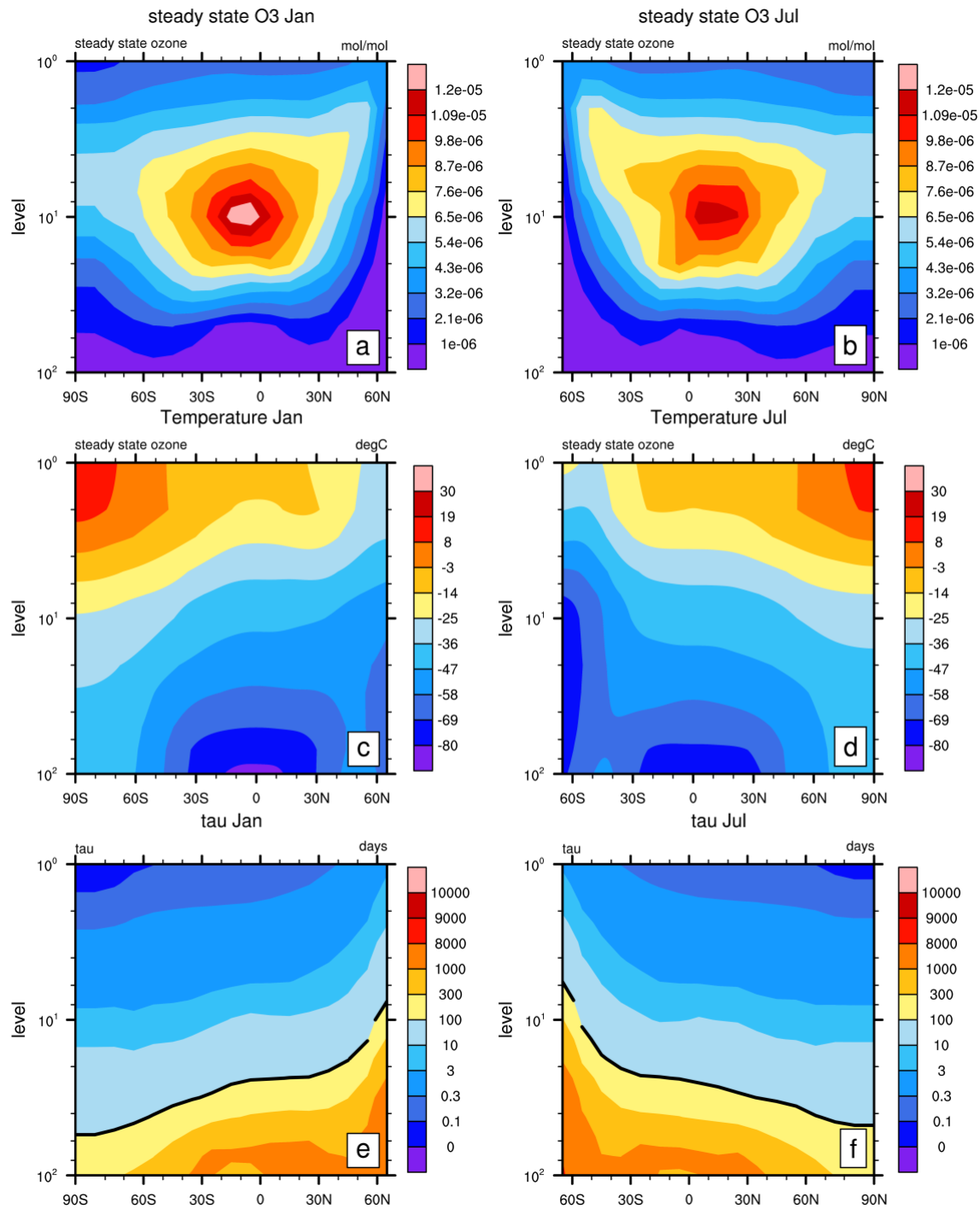
Figure 2 The (a, b) steady state ozone (mol/mol) derived using Linoz-v2 on E3SMv2
temperature, (c, d) ERA5 temperature (°C), (e, f) photochemical relaxation time τ (days), and for
January and July. The thick black line in (c, d) denotes the 300 value-line.
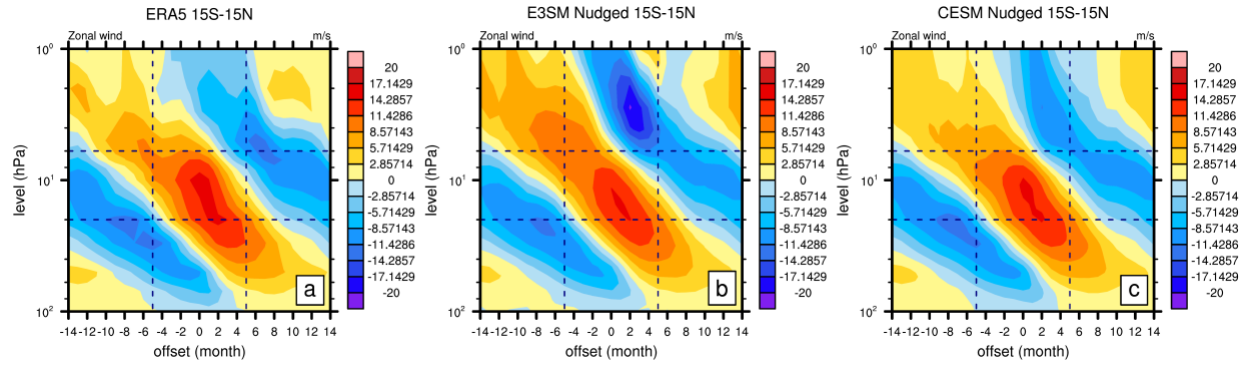
Figure 3 Pressure-time cross-section of the tropical (15°S-15°N) zonal wind anomaly (m/s) as function of QBO phase for (a, d) ERA5, (b, e) E3SMv2, (c, f) CESM2 for 1979-2020. 0 is centered on the month when QBO index shifts from QBOe to QBOw (determined by when current QBO index<0 and next QBO index>0). The QBO phase is determined by 5S-5N average of the zonal wind.
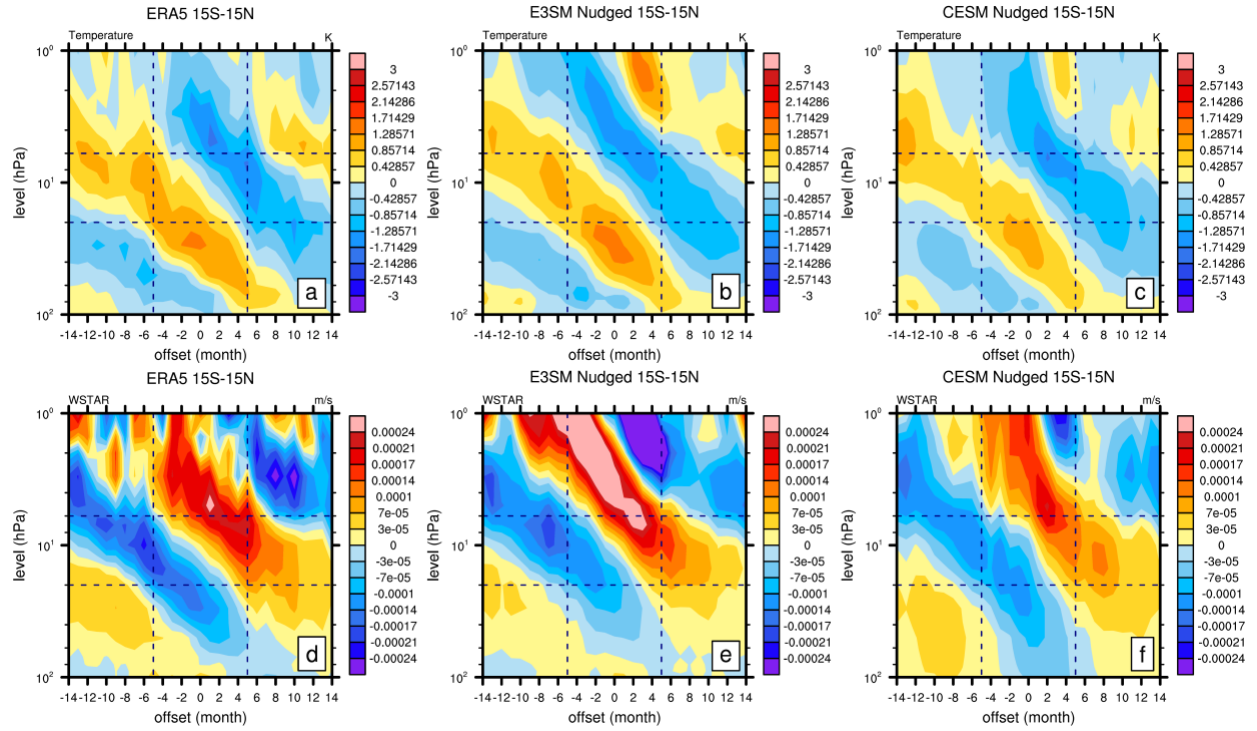
Figure 4 Pressure-time cross-section of the tropical (15°S-15°N) temperature (K) and $\underline{w}^*$ anomaly (Transformed Eulerian Mean residual vertical transport, m/s) as function of QBO phase for (a, d) ERA5, (b, e) E3SMv2, (c, f) CESM2 for 1979-2020. 0 is centered on the month when QBO index shifts from QBOe to QBOw (determined by when current QBO index<0 and next QBO index>0). The QBO phase is determined by 5S-5N average of the zonal wind.

938
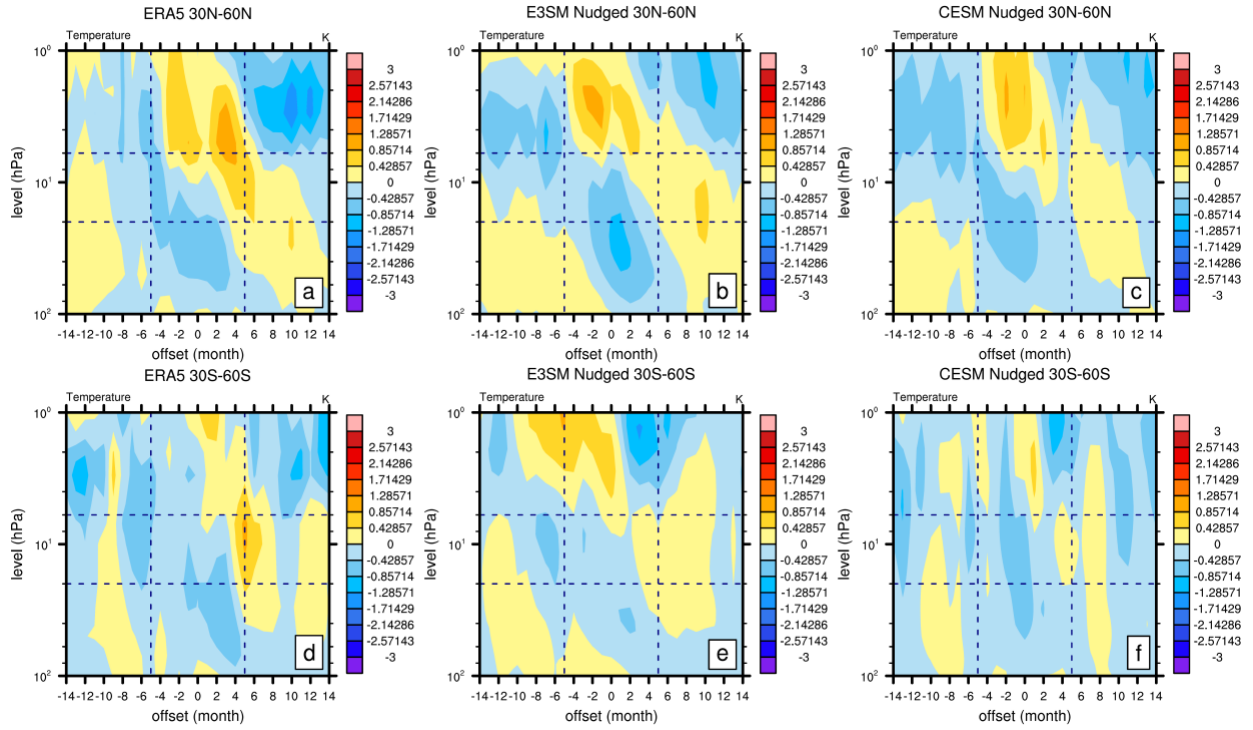
Figure 5 As in Figure 4, but for the extra-tropical (30°N-60°N/30°S-60°S) temperature anomaly

(K) as function of QBO phase for (a, d) ERA5, (b, e) E3SMv2, (c, f) CESM2 for 1979-2020.

941

942

943
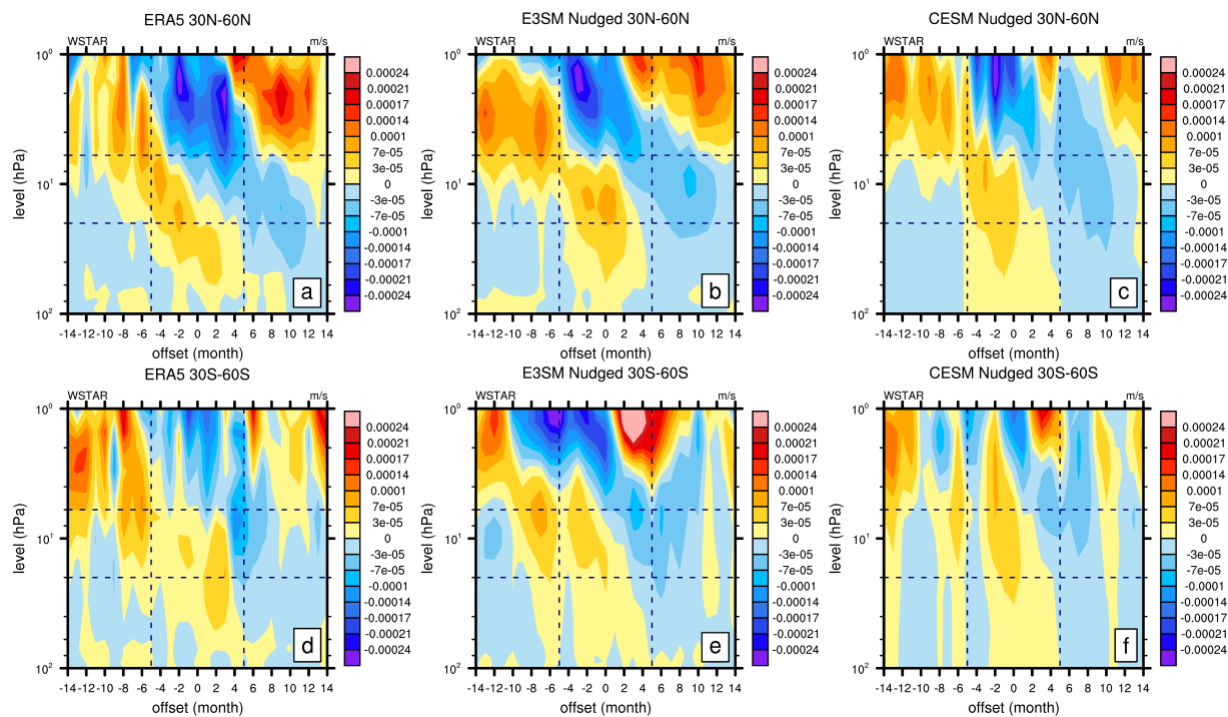
Figure 6 As in Figure 4, but for the extratropical (30°N-60°N/30°S-60°S) $\underline{w}^*$ anomaly (m/s) as

function of QBO for (a, d) ERA5, (b, e) E3SMv2 nudged, (c, f) CESM2 nudged for 1979-2020.

946

947
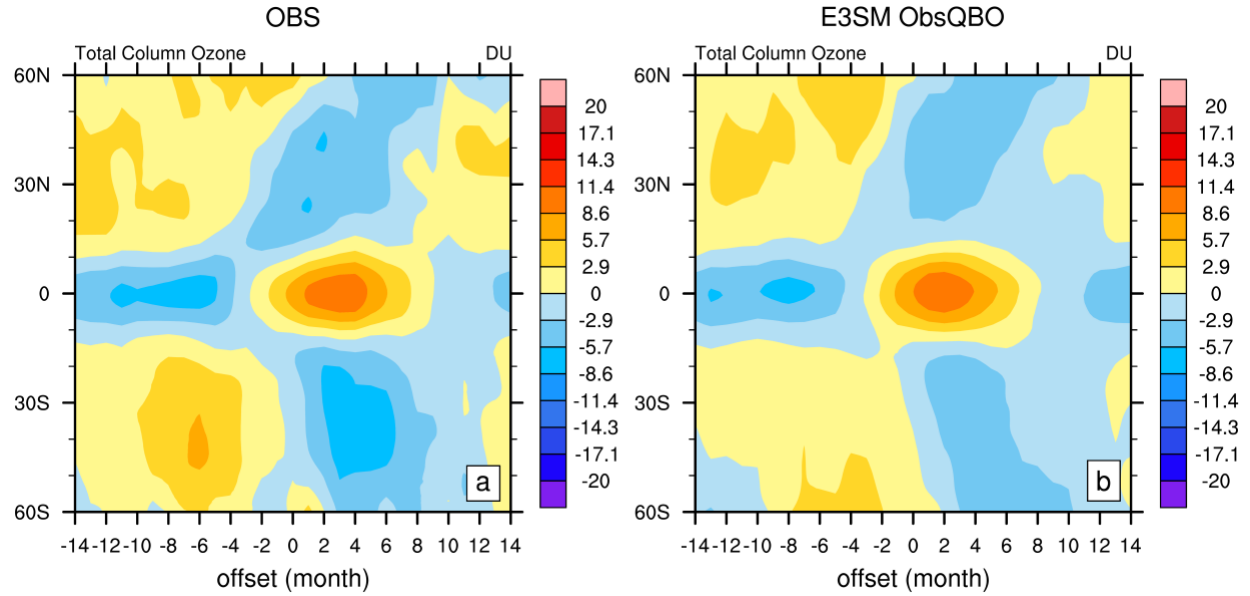
Figure 7 As in Figure 4, but for time-latitude map of Total column ozone (TCO, Dobson Unit) anomaly (relative to 1979-2020 mean) composites as function of QBO phase (determined by NLPCA QBO index) for (a) OBS (Multi-Sensor Reanalysis version 2), (b) E3SMv2 nudged simulation for 1979-2020.
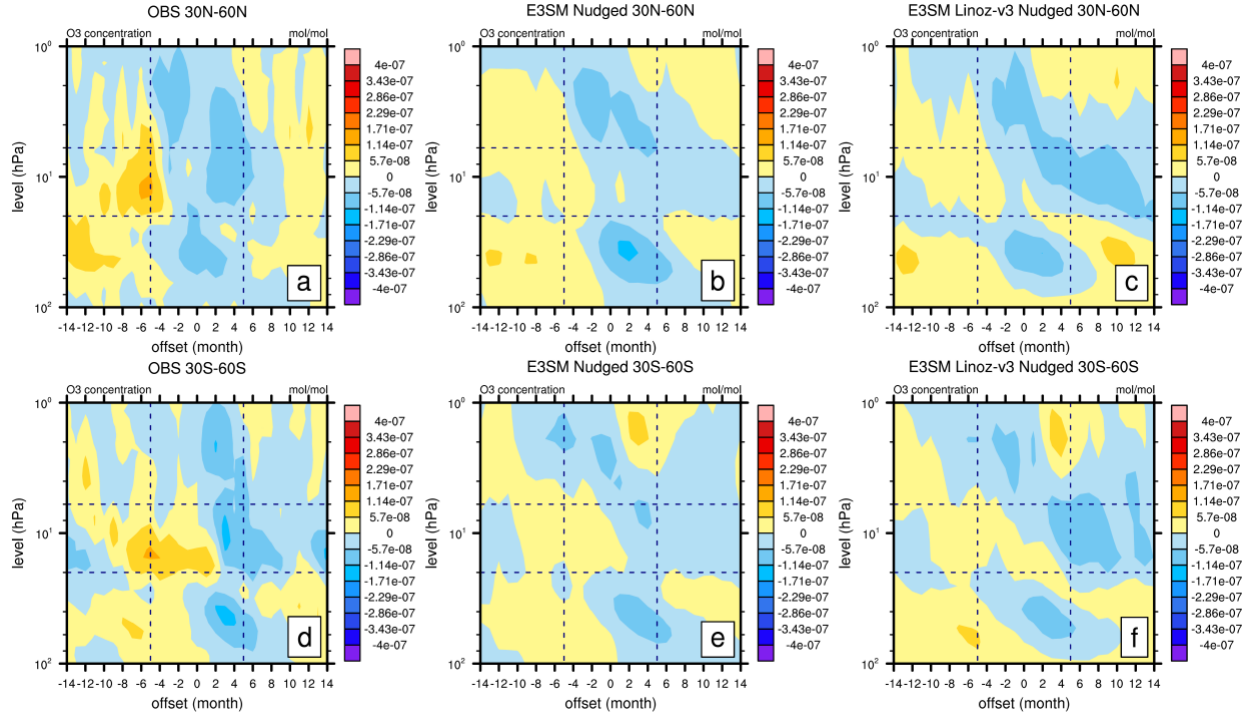
955
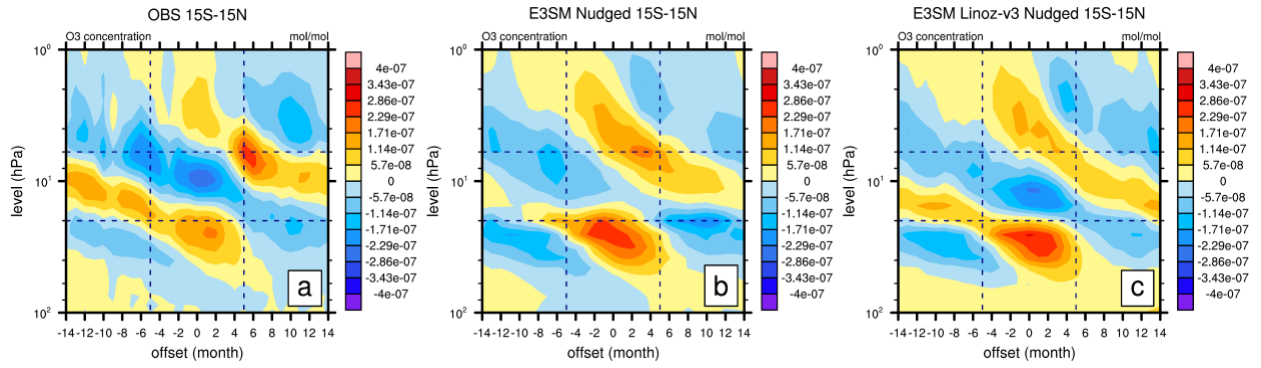
Figure 8 As in Figure 4, but for the tropical (15°S-15°N) ozone concentration anomaly (mol/mol)

as function of QBO phase for (a) Observation (Concentration Monthly Zonal Mean), (b)

E3SMv2 nudged simulation, (c) E3SMv2 Linoz-v3 nudged simulation for 1979-2020.

959

960

961   Figure 9 As in Figure 4, but for the extratropical (30°N-60°N/30°S-60°S) ozone concentration

962   anomaly (mol/mol) as function of QBO phase for (a, d) OBS (CMZM), (b, e) E3SMv2, (c, f)

963   CESM2 for 1979-2020. E3SMv2 Linoz-v3 nudged simulation is produced using nudged

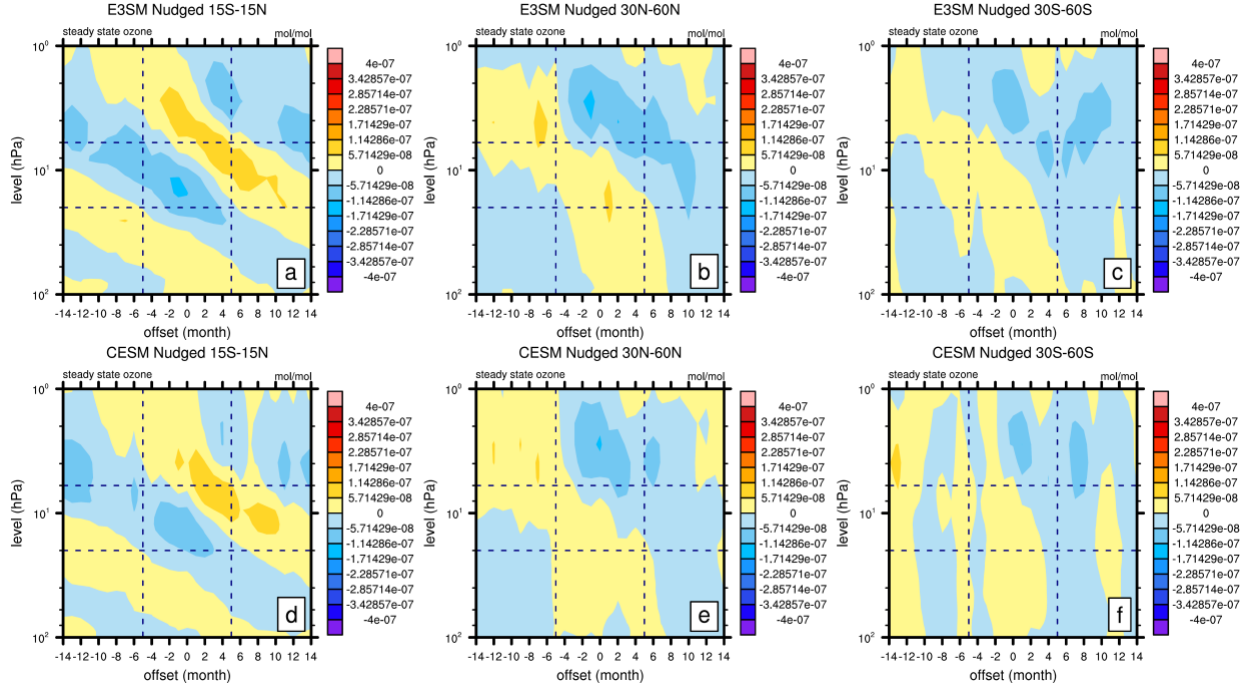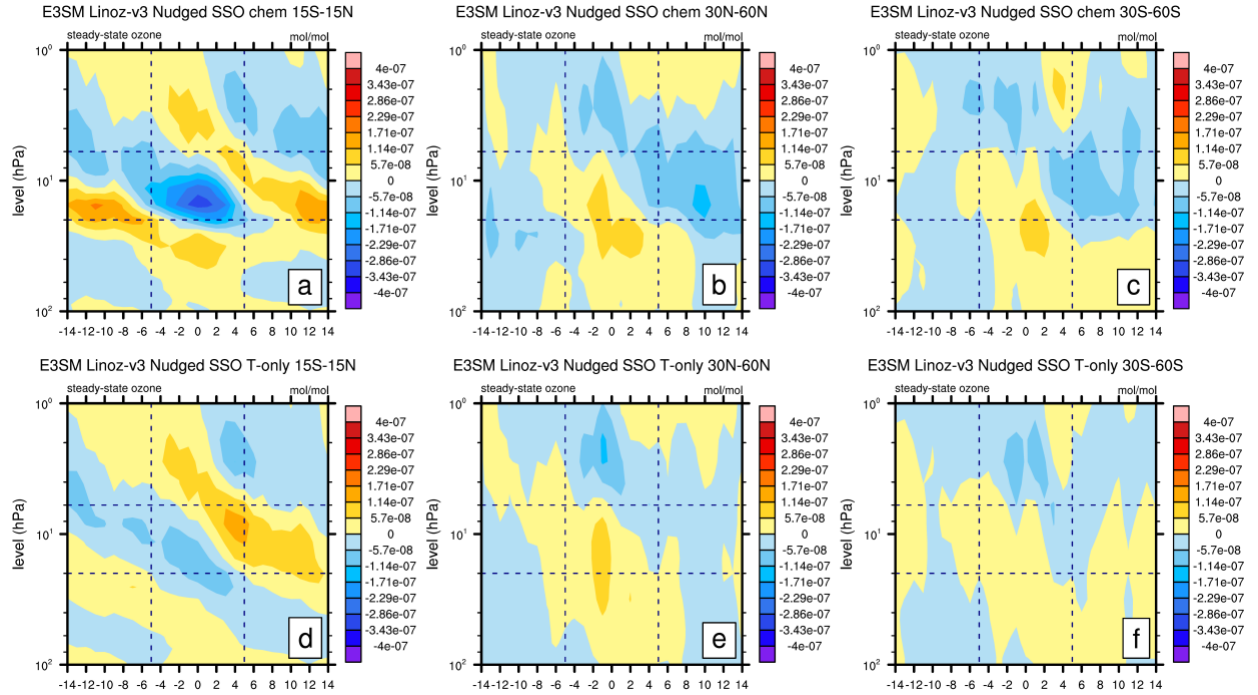964   E3SMv2 with stratospheric chemistry replaced with Linoz-v3.

965

966

967

968 Figure 10 As in Figure 4, but for the tropical (15°S-15°N) and extratropical (30°N-60°N/30°S-

969 60°S) steady state ozone anomaly (mol/mol) as function of QBO phase for (a) E3SMv2 and (b)

970 CESM2 for 1979-2020.

971

972

973 Figure 11 As in Figure 4, but for the tropical (15°S-15°N) and extratropical (30°N-60°N/30°S-

974 60°S) steady state ozone anomaly (mol/mol) as function of QBO for E3SMv2 Linoz-v3 Nudged

975 simulation using (a, b, c) Linoz-v3 chemistry (NO$_y$-N$_2$O-CH$_4$-H$_2$O), (d, e, f) temperature only for
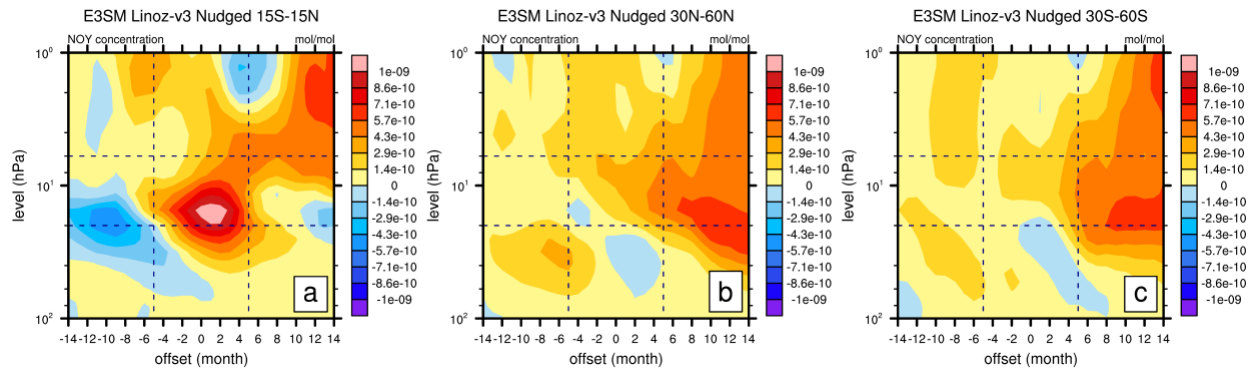
976 1979-2020.

977

978

979 Figure 12 As in Figure 4, but for the tropical (15°S-15°N) and extratropical (30°N-60°N/30°S-

980 60°S) NO$_y$ anomaly (mol/mol) as function of QBO (a, b, c) E3SMv2 Linoz-v3 for 1979-2020.
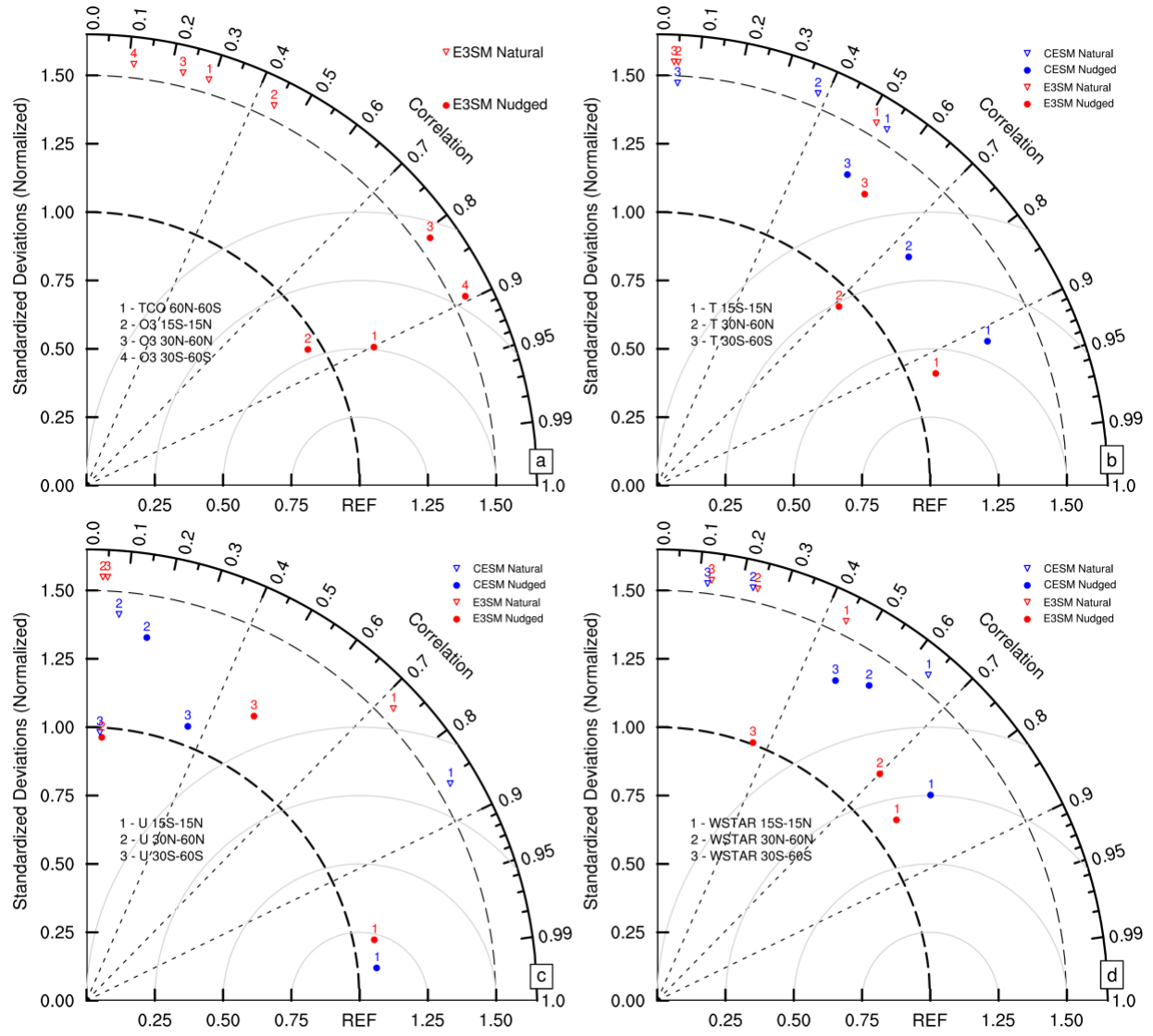
981

982

Figure 13 Taylor diagram of the E3SMv2/CESM2 simulation for various datasets for 1979-2020. (a) The area-weighted total column ozone (60°S-60°N, DU) and pressure-time cross-sections of ozone concentration (15°S-15°N, 30°N-60°N, 30°S-60°S, mol/mol) anomalies with OBS (MSR and CMZM), respectively. (b) The area-weighted pressure-time cross-sections of temperature (15°S-15°N, 30°N-60°N, 30°S-60°S, K) anomalies with ERA5. (c) The area-weighted pressure-time cross-sections of zonal wind (15°S-15°N, 30°N-60°N, 30°S-60°S, m/s) anomalies with ERA5. For pattern correlations, the cross-sections are weighted by pressure layer thickness. On all Taylor diagrams, the model standard deviations are normalized by dividing the standard deviations of the reference.

41